Integration of Mars Global Surveyor Observations of the MY 25 Global Dust Storm on Mars: Implications for Atmospheric Dynamics and Modeling

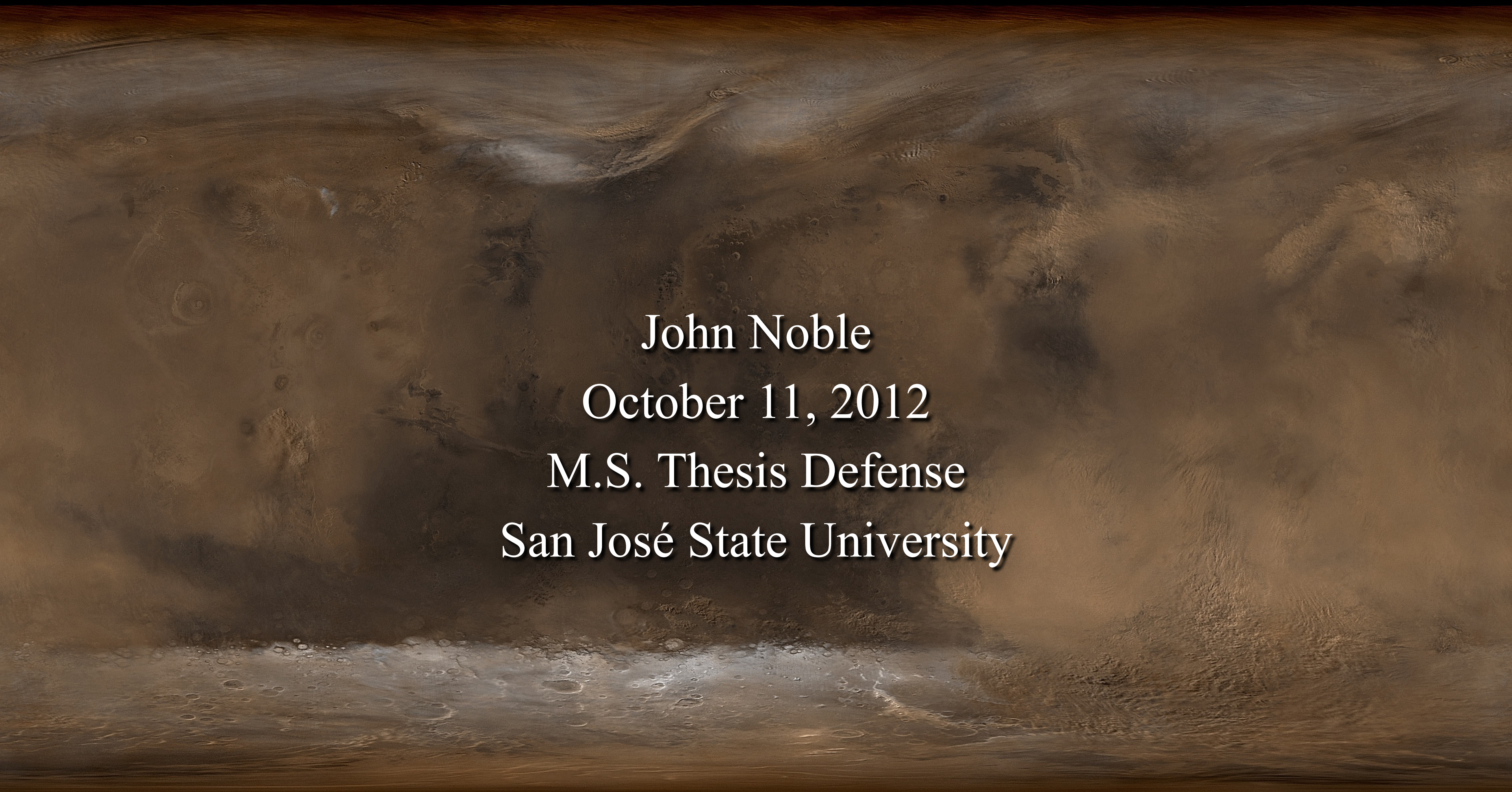

John Noble

October 11, 2012

M.S. Thesis Defense

San José State University

Outline

1. Motivation
2. Problem statement
3. Mars overview
4. Results
5. Conclusions

Motivation

1. Fundamental geophysical research is required to better understand the Martian atmosphere.

2. Global dust can be used as a tracer to reveal underlying dynamical processes, and improve our understanding of regional and global circulation components.

3. The Martian atmosphere serves as a planetary laboratory to test and advance our understanding of geophysics and comparative planetary atmospheric science.

4. Comprehensive knowledge of the Martian atmosphere is necessary to ensure the safety and success of future robotic and human missions.

Nomenclature

- GDS – Global dust storm
- MGCM – Mars general circulation model
- MGS – Mars Global Surveyor
- MY – Mars year
  - MY 25 GDS started in June 2011

Problem statement

- The environmental causes and dynamical mechanisms responsible for GDS initiation, expansion, decay, and interannual frequency are not fully understood, posing fundamental unsolved problems in Martian atmospheric science.

- GDS seasonal occurrence suggests the presence of climatic and environmental factors, yet interannual variability suggests that initiation and expansion mechanisms are not solely seasonal in character.

Objectives

Better understand and characterize the dynamical processes responsible for MY 25 GDS initiation and expansion, specifically examining the following questions:

1. Which circulation components were involved in storm onset and evolution?

2. How did the temperature and dust opacity fields evolve together?

3. Do MGS data show interannual variability that suggests why a GDS formed in MY 25 and not in MY 24 or 26?

Earth and Mars comparison

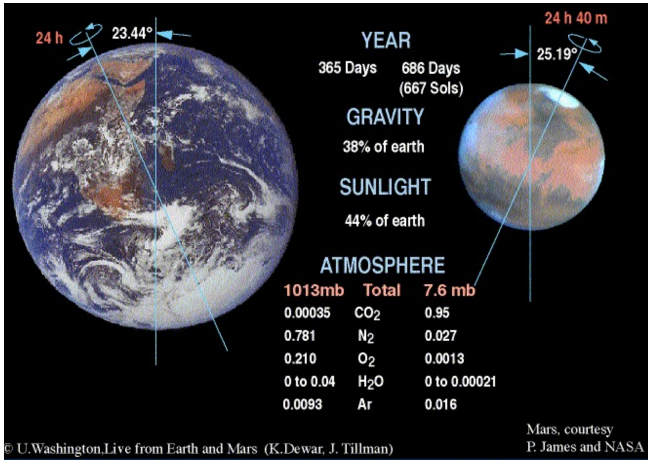

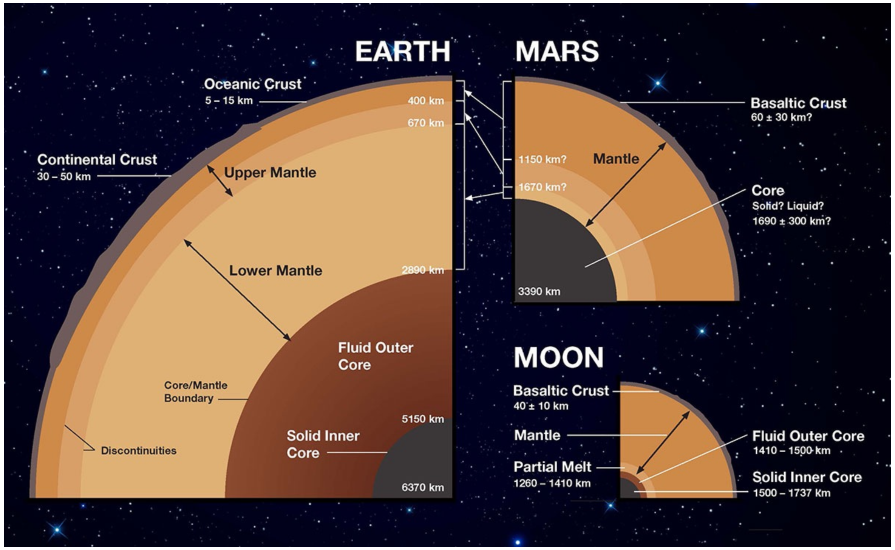

Martian orbit, time, and seasons

L_s – Areocentric longitude; an angular measure of Mars' orbit relative to the sun.

- Used to measure seasons.
- SH seasons are reversed, SH spring equinox: L_s=180º.

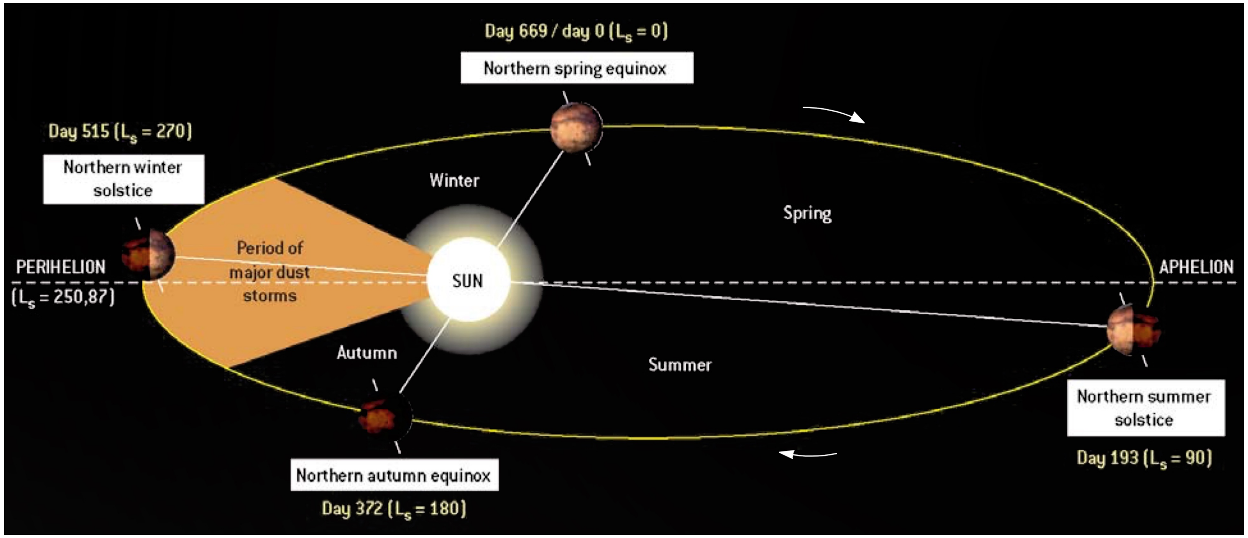

Sol – Martian day (24.6 Earth hours)

Mars year (MY), consists of 687 sols

- MY 25 GDS started at L_s = 184º (June 2011).

General circulation & atmospheric processes

General circulation of the lower atmosphere at (a) equinoxes, and (b) solstices (Haberle 1997). (c) Atmospheric processes (Haberle 2003)

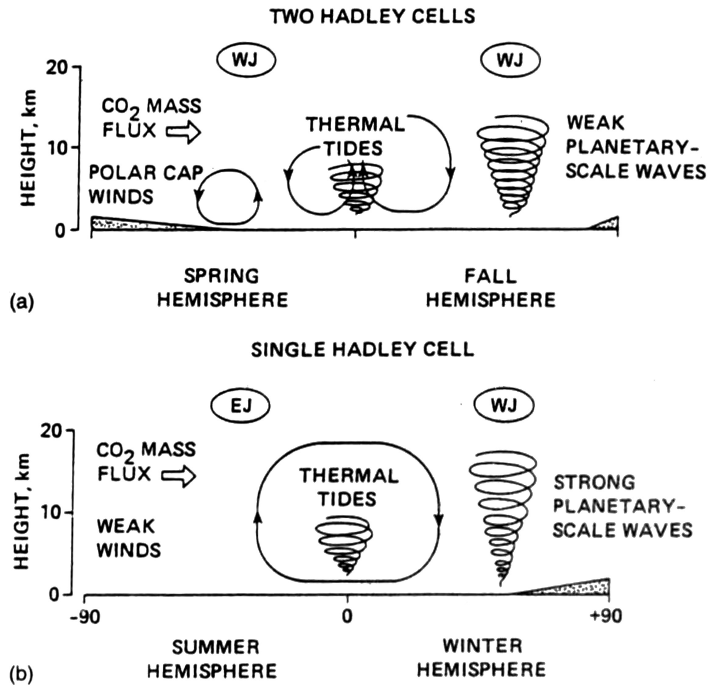

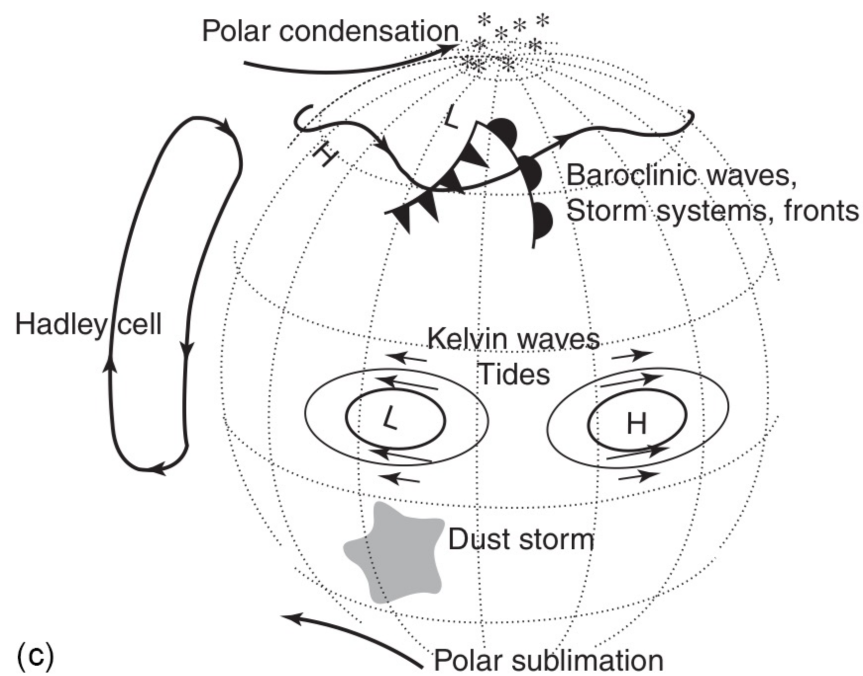

Atmospheric pressure levels & height

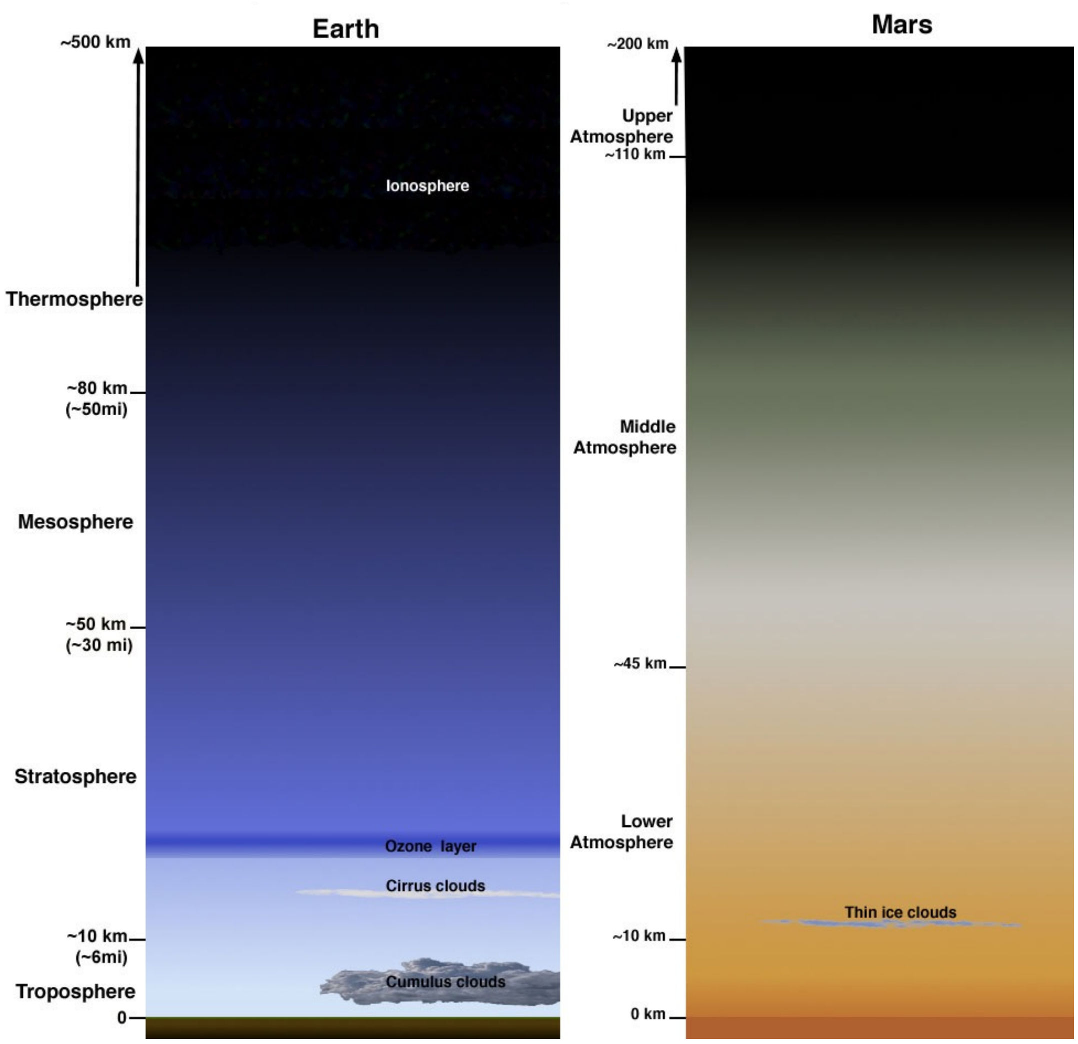

Pressure level (hPa)	~Log pressure height (km) $z^* \equiv H \ln(p_r / p)$	TES nadir height description
0.01	70.4	
0.015	64.9	
0.025	59.4	
0.041	54.0	
0.068	48.6	
0.11	43.4	Upper
0.18	38.0	Upper
0.3	32.5	Middle
0.5	27.0	Middle
0.83	21.5	Middle
1.36	16.2	Middle
2.24	10.8	Lower
3.7	5.4	Lower
6.1	~0 (mean sfc.)	

Planetary & atmospheric parameters for Mars and Earth

Parameter	Mars	Earth
Mass (kg)	6.46×10^{23}	5.98×10^{24}
Semi-major axis, ($\times 10^6$ km) (AU)	227.9 1.52	149.6 1.0
Orbital eccentricity	0.093	0.017
Planetary obliquity (°)	25.19	23.93
Rotation rate, $\Omega\left(10^{-5}\cdot \mathrm{s}^{-1}\right)$	7.088	7.294
Solar day (s)	88,775	86,400
Year length (Earth days)	686.98	365.24
Equatorial radius, r_{eq} (km)	3,394	6,369
Surface gravity, $g\left(\mathrm{m}\cdot \mathrm{s}^{-2}\right)$	3.72	9.81
Surface air pressure, p (hPa)	6.1*	1013
Constituents of lower (<120 km) atmosphere (molar ratio, %)	CO_2 (95) N_2 (2.7) ^{40}Ar (1.6) O_2 (0.13) H_2O (0.03)*	CO_2 (0.037) N_2 (77) ^{40}Ar (0.9) O_2 (21) H_2O (0–4)
Solar flux ("solar constant"), S_0 $\left(\mathrm{W}\cdot \mathrm{m}^{-2}\right)$	589	1367
Radiative equilibrium temperature, T_e (K)	210	256
Scale height, $H_p = \frac{RT_e}{g}$ (km)	10.8	7.5
Gas constant, $R\left(\mathrm{J}\cdot \mathrm{kg}^{-1}\cdot \mathrm{K}^{-1}\right)$	192	287
Specific heat at constant pressure, $c_p\left(\mathrm{J}\cdot \mathrm{kg}^{-1}\cdot \mathrm{K}^{-1}\right)$	831	1000
Dry adiabatic lapse rate, $\Gamma_d\left(\mathrm{K}\cdot \mathrm{km}^{-1}\right)$	4.5	9.8
Mean lapse rate of lowest scale height, Γ (K km^{-1})	2.5	6.5
Buoyancy (Brunt–Väisälä) frequency, N (10^{-2} s^{-1})	~0.6	1.12
Bulk radiative timescale, τ_r (10^5 s)	2	40
Typical zonal wind at jet level, $U\left(\mathrm{m}\cdot \mathrm{s}^{-1}\right)$	80	30

* Variable with season. $\bar{p} \approx 6.1$ hPa. Spatial and temporal range $\approx$ 4–10 hPa

(Haberle 2003; Leovy 2001; Owen 1992; Read and Lewis 2004; Zurek *et al.* 1992)

Mineral aerosols

- Mineral aerosols, hereafter dust (1–2 μm radius)
- Dynamically, radiatively, and thermally coupled with the atmosphere
- Influence weather, climate, and atmospheric circulation
- Agents of geological change
- Absorb and scatter incoming solar radiation
- Absorb and emit IR radiation
- IR radiation emitted from dust is absorbed and re-emitted by CO_2, which in turn causes warming.
- Dust optical depth has large variability:

$$\sigma_\lambda = \sec\theta \, k_\lambda \int_0^x \rho \, dz$$

Global dust storms

- Dust storms change the thermal structure of the atmosphere by:
  - lowering temperatures near the surface due to absorption of incoming solar radiation.
  - raising temperatures aloft by emitting IR radiation.

- This subsequently affects the pressure, winds, and ultimately general circulation.

- Movement and redistribution of dust affects albedo.

Mars Global Surveyor datasets

- Thermal emission spectrometer (TES)
  - Temperature – surface and atmospheric
  - Dust optical depth (column abundance)
- Fast Fourier Synoptic Mapping (FFSM)
  - Spectral analysis method that creates synoptic maps from asynoptic data (Barnes)
- Mars Orbiter Camera (MOC)
  - Daily global maps (DGM) of 12–13 swaths
- Mars Horizon Sensor Assembly (MHSA)
  - Temperature; 10–40 km avg – broad weighting function
  - Contains continuous measurements

Mars Global Surveyor

Martian geography and place names

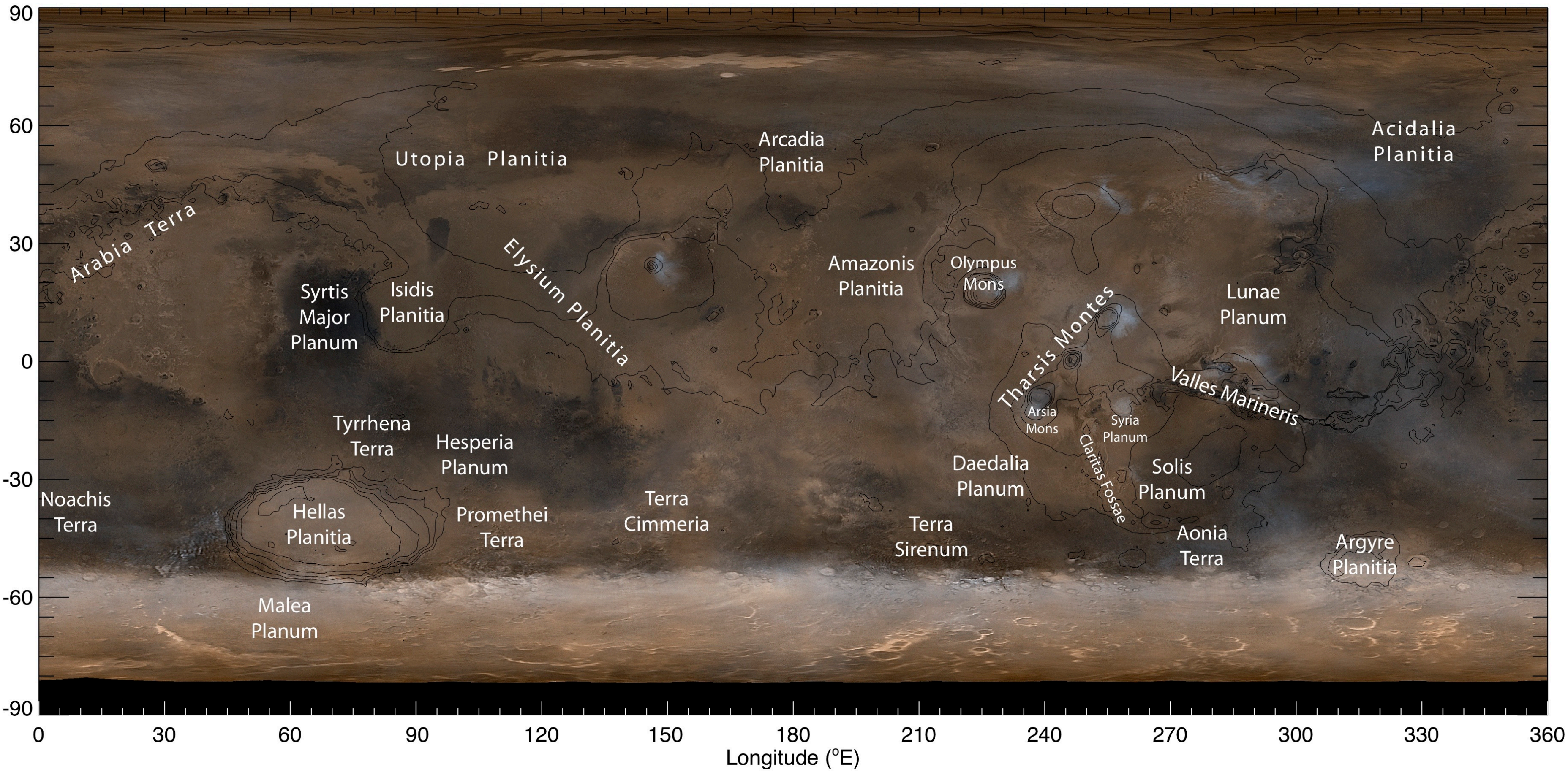

MOC DGM – 12 swaths of 2 pm images

Results

1. GDS Overview

2. Precursor phase
   - FFSM eddies and MOC–observed dust storms

3. Expansion phase
   - Wave one evolution

4. Dust height estimates

5. Synthesized dust maps

Results will be presented in 15 slides

MY 25 global dust storm evolution

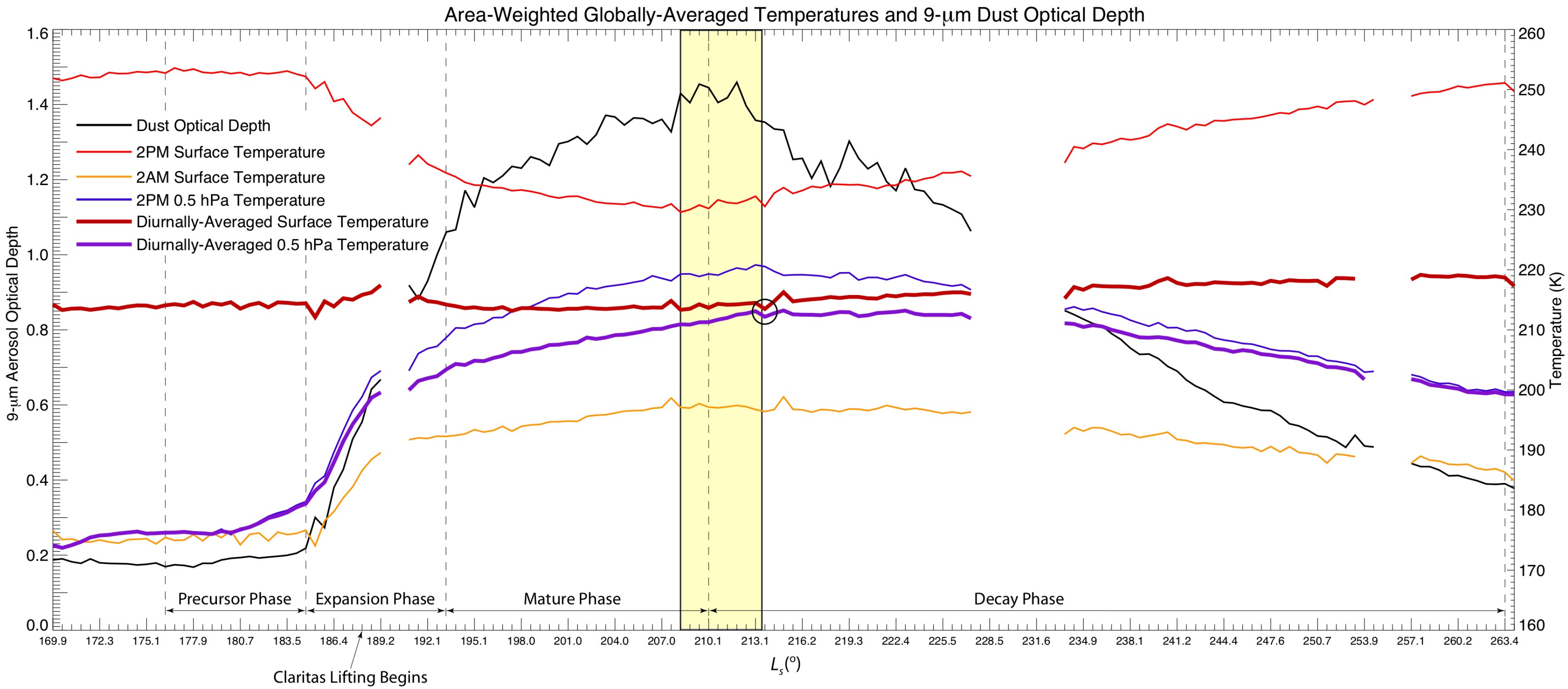

GDS phases

Precursor: L_s=176.2–184.6°

Expansion: L_s=184.7–193°

Mature: L_s=193–210°

Decay: L_s=210–263°

- All temperatures reach extrema from L_s=208–213°.
- Diurnally averaged surface and 0.5 hPa temperatures are nearly isothermal at L_s=213°.

R1

Precursor phase

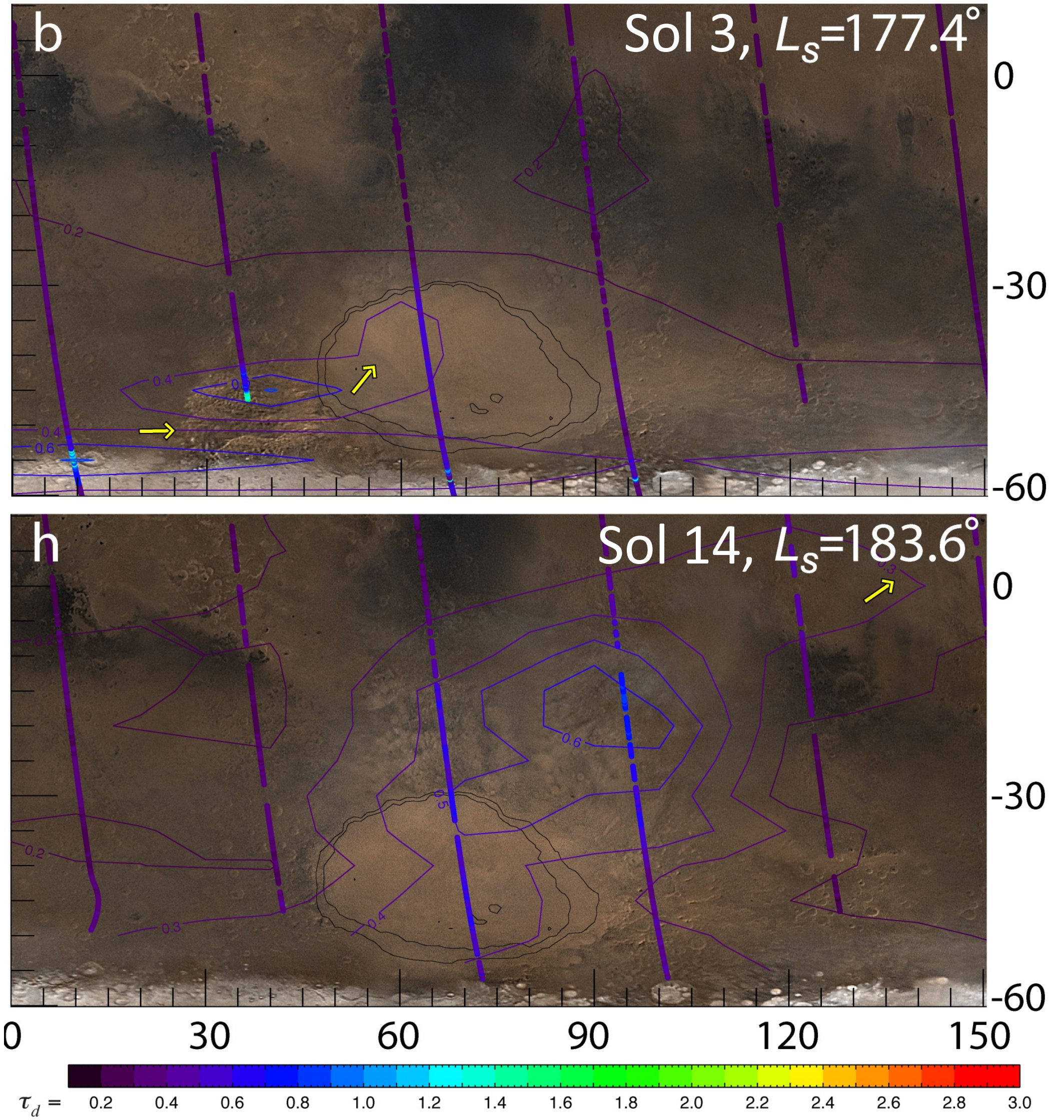

Cap-edge dust storm
SW Hellas

Dust transport
NE Hellas

R2

TES FFSM eddies and MOC-observed storms, 3.7 hPa, 60° S, MY 25

R3

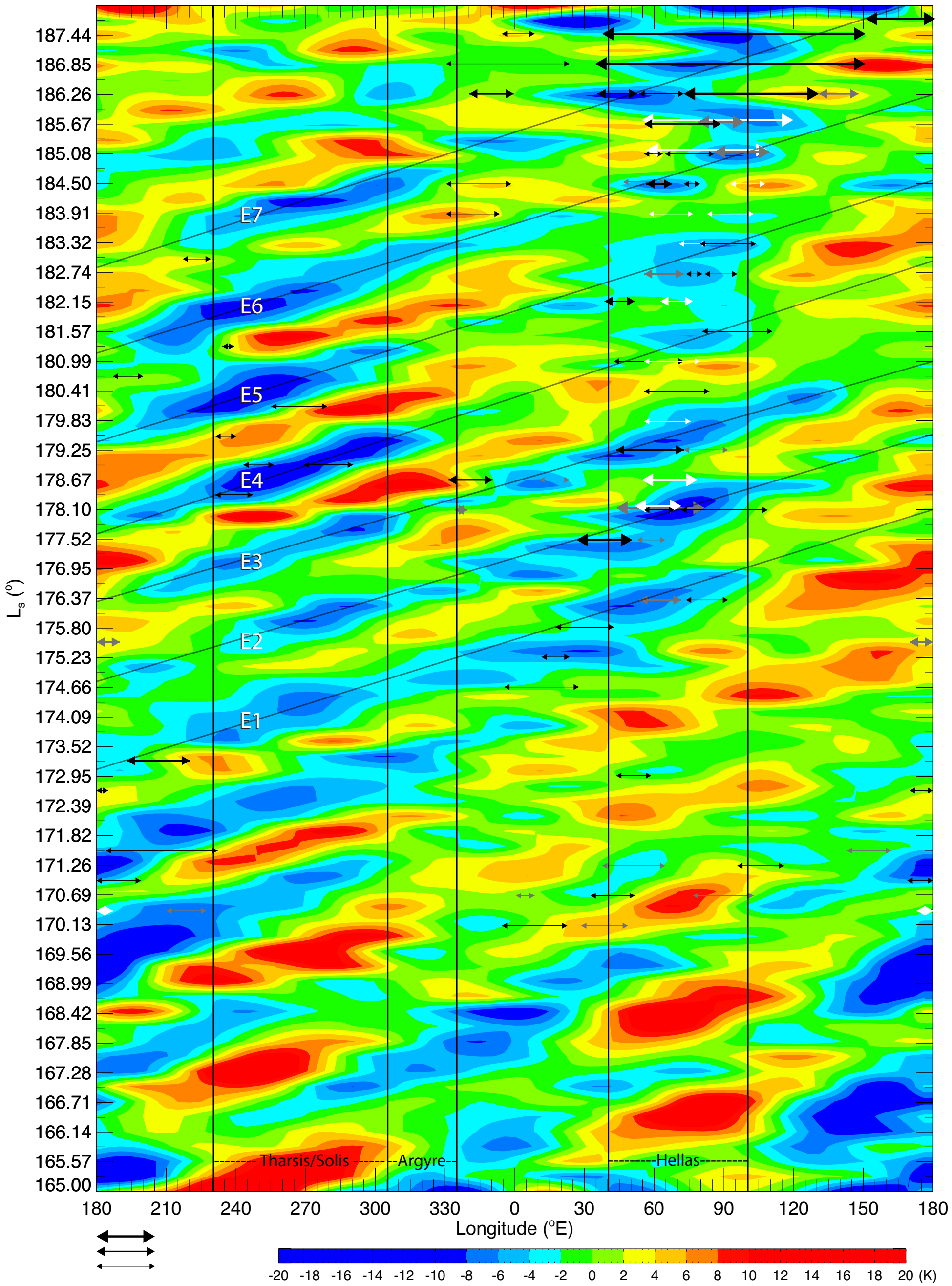

- Six eastward-traveling baroclinic eddies triggered the precursor storms due to the enhanced dust lifting associated with their low-level wind and stress fields.
- Increased opacity and temperatures from dust lifting associated with E1–E3 enhanced thermal tides which supported further storm initiation and expansion out of Hellas.
- E7 contributed to expansion on L_s=186.3°.
- Northward storm evolution is due in part to northward winds associated with cold fronts. Cold fronts are a characteristic of baroclinic eddies, and in the SH, baroclinic eddies cause northward winds.

Arrow colors = storm latitude

White	**25–35° S**
Grey	**35–45° S**
Black	**45–75° S**

TES FFSM eddies on MOC DGMs, 3.7 hPa, Hellas quadrant

R4

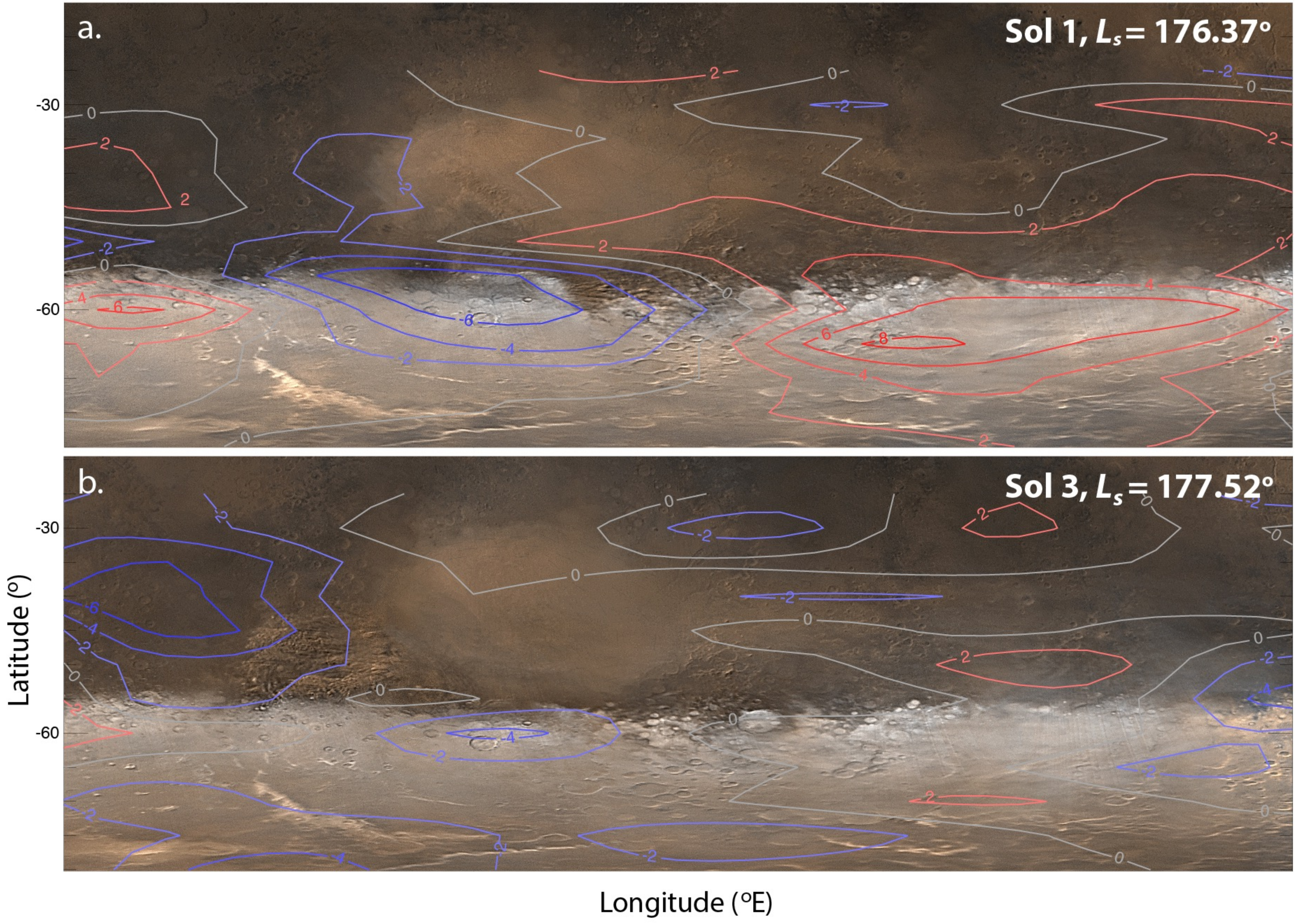

FFSM eddies in Hellas, 60° S

Change of eddy structure with height indicates that these are not barotropic eddies, and suggests that they are eastward propagating baroclinic eddies.

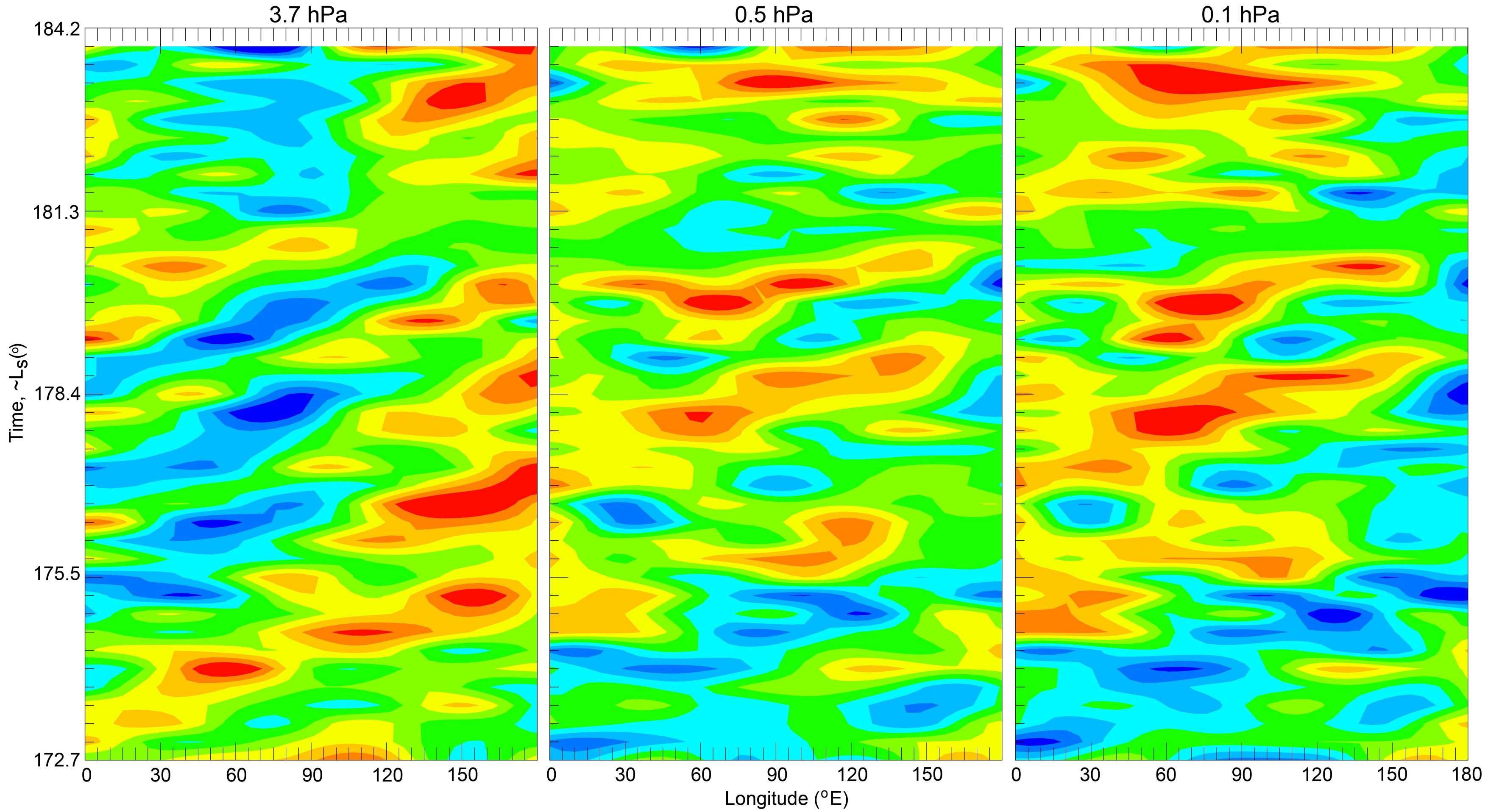

R5

TES FFSM eddies and MOC-observed storms, 3.7 hPa, 60° S, MY 24

R6

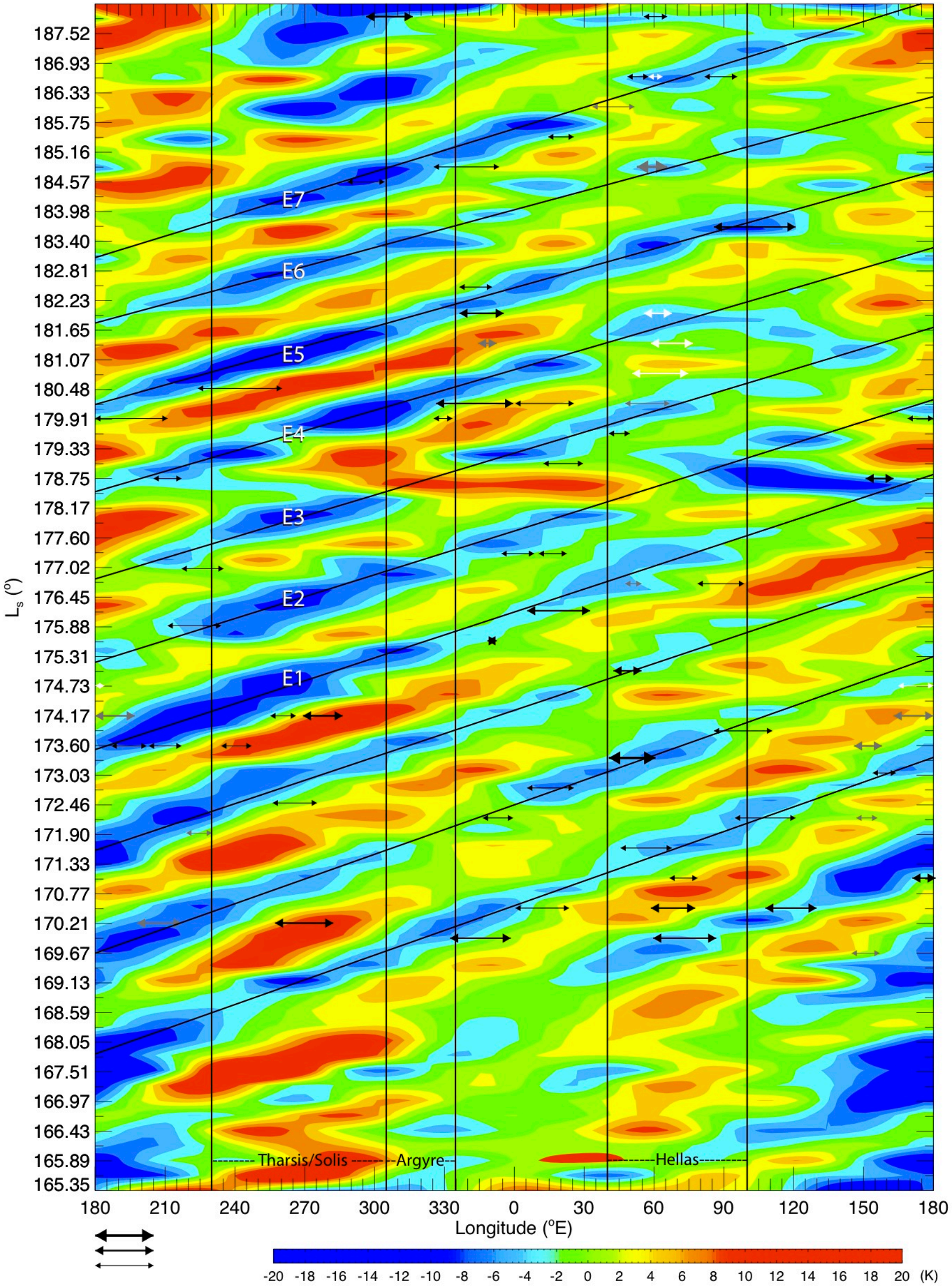

Major cap-edge storms south of Hellas occur less frequently in MY 24 compared to MY 25

L_s=169.9° large cap-edge storms occurred east of Argyre at 345° E and within Hellas at 80° E.

L_s=173.3° a large storm emerged west of Hellas, followed by a smaller one in SW Hellas three sols later at L_s=175.1°.

L_s=180.2° a large cap-edge storm developed between Argyre and Hellas (~330–25° E), along with a storm in NW Hellas.

L_s=183.5°, dust clouds with a rippled appearance were visible along the cap edge SE of Hellas.

Arrow colors = storm latitude

White	**25–35° S**
Grey	**35–45° S**
Black	**45–75° S**

TES FFSM 3.7 hPa cold anomaly amplitudes vs. time, Hellas (45–90° E, 50–60° S), MY 24–26

We hypothesize that the sustained series of high-amplitude eddies in MY 25 was a factor in GDS interannual variability.

MY 24: 2 eddies (E5 & E7) colder than –3.5 K
MY 25: All eddies colder than –3.5 K
MY 26: 1 eddy colder than –3.5 K

These eddies would have had higher-amplitude low-level wind and stress fields associated with them, and could have led to more dust lifting.

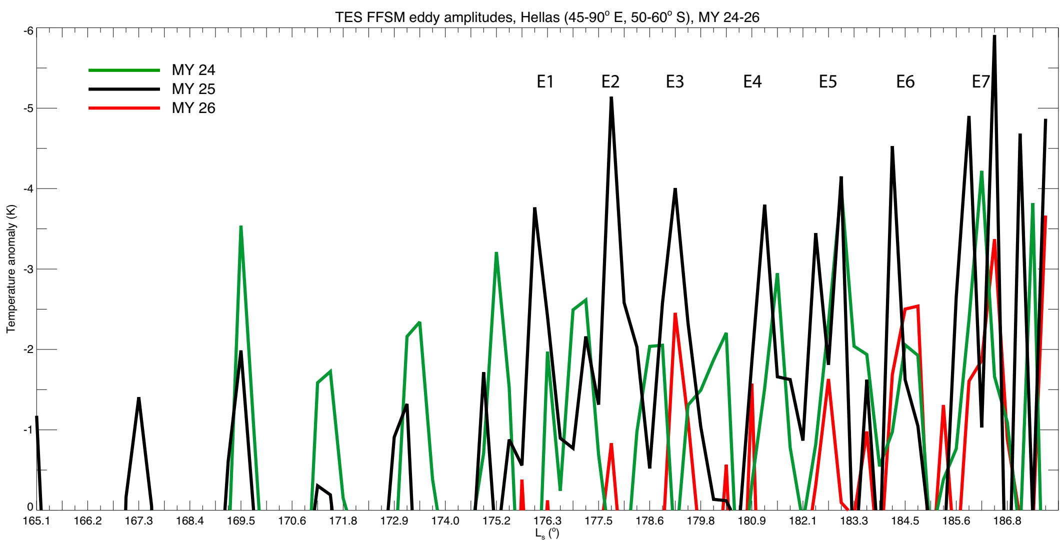

Constructive interference of MY 25 eddies and other circulation components including:

- sublimation flow
- anabatic winds (upslope)
- diurnal tides
- dust-induced thermal tides

may have led to the initiation and expansion of precursor storms.

Constructive interference increases surface stresses capable of lifting dust (through the wind field)

R7

Phase speed and periodicity

Year (MY)	Global phase speed, c, (m s^{-1})	Period, P (sols)
24	14.3	2.7
25	13.8	2.9
26	13.7	3.1

TES FFSM 3.7 hPa eddy power spectra, Hellas, L_s=165–188°

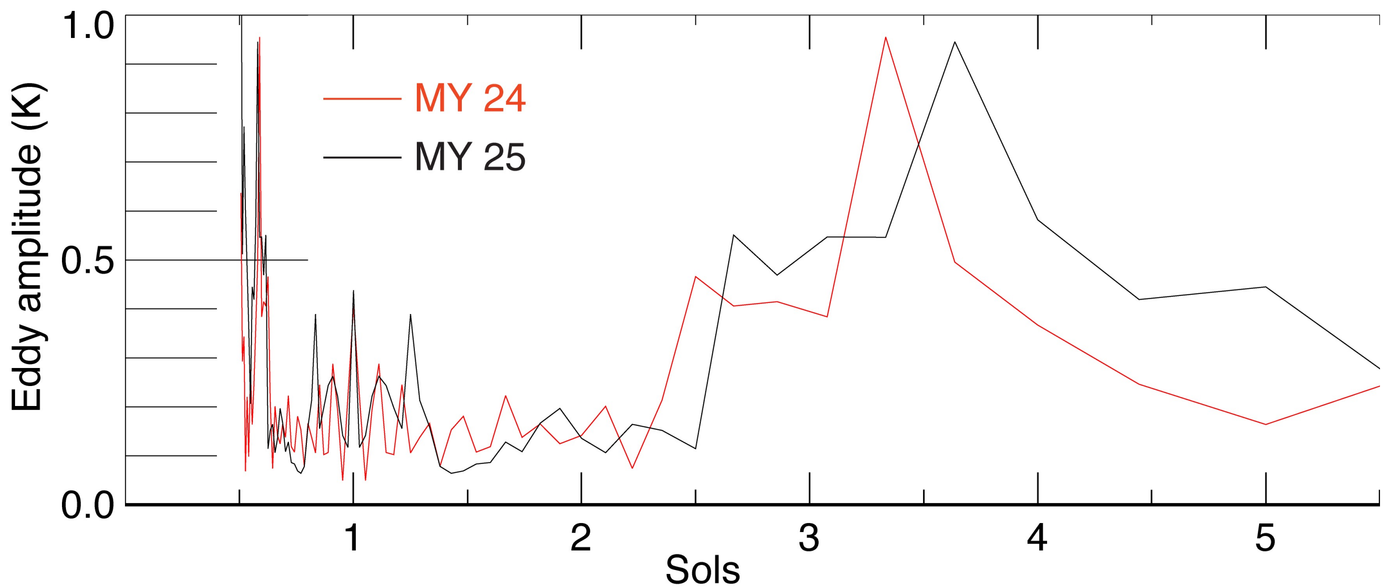

R8

Expansion phase

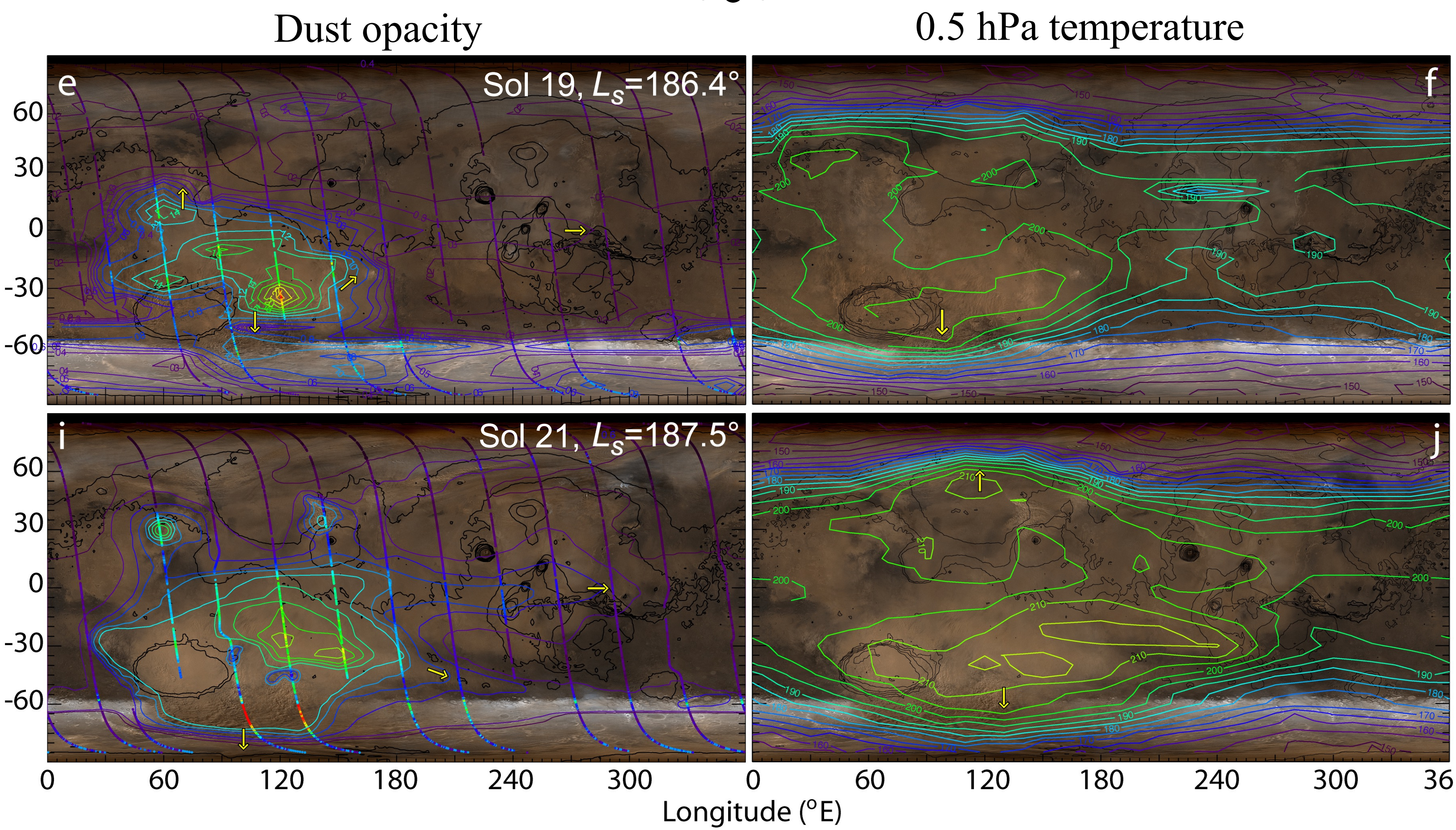

- Dust transport to the NE, E, & S of Hellas
- Westerly flow along the equator
- Wave one maximum amplitude at L_s=187.5°

R9

Time histories of opacity & temperature L_s=180–188.7°

a) 60–90° E
60–30° N

b) 85–110° E
70–65° N

Adiabatic (compressional) heating from descending branch of enhanced Hadley cell

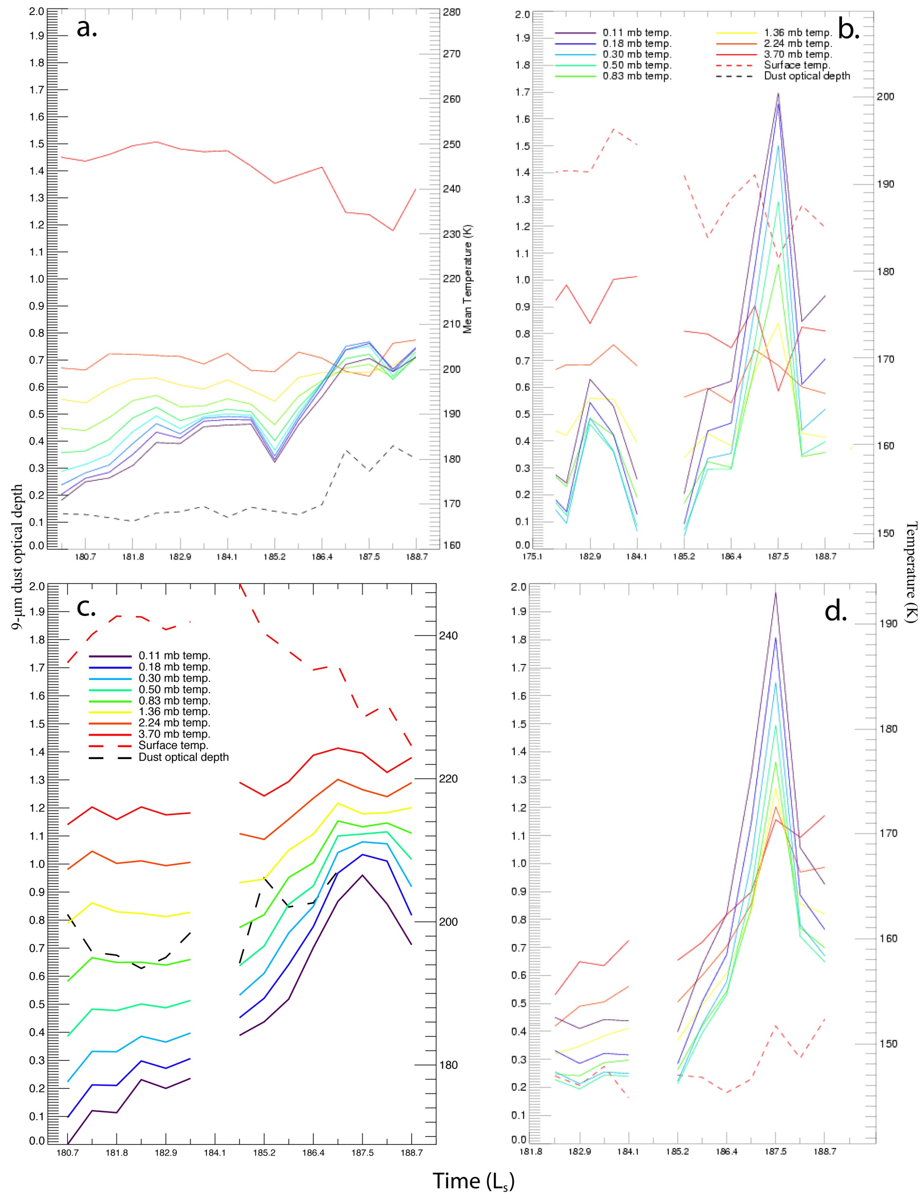

c) 60–85° E
40–45° S

d) 90–115° E
80–85° S

R10

Expansion phase

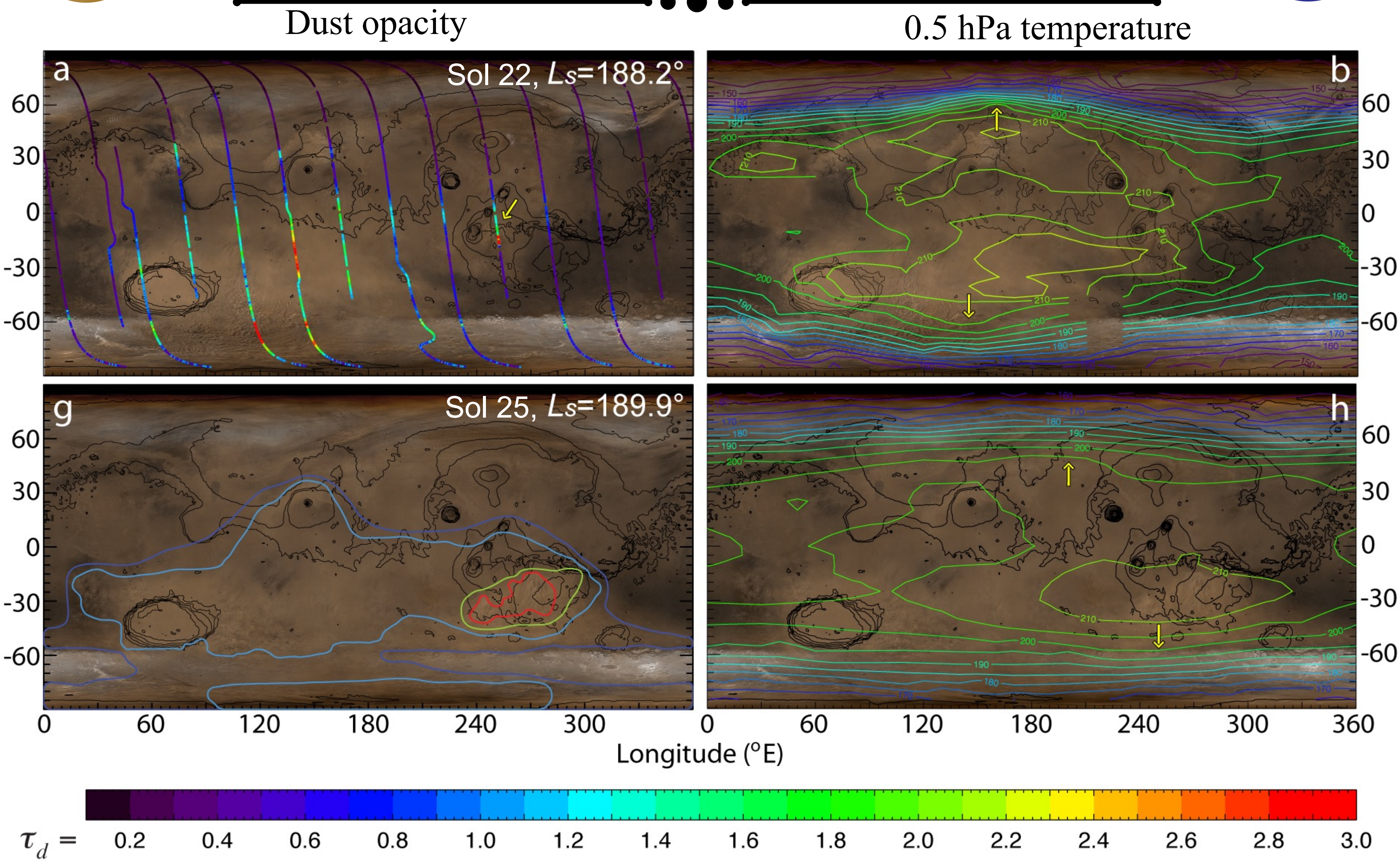

R11

Zonal evolution of storms & 0.5 hPa NH & SH wave 1 warm peaks

We hypothesize that wave one amplification during the precursor phase was primarily due to

- a longitudinally-varying response to SH dust heating.
- subsequent longitudinally-varying enhancement of the Hadley circulation.

SH dust-induced heating strengthened the equatorial rising branch of the Hadley circulation, leading to:

- intensification of the descending branches.
- subsequent increased dynamically-induced adiabatic (compressional) heating at high latitudes in both hemispheres.

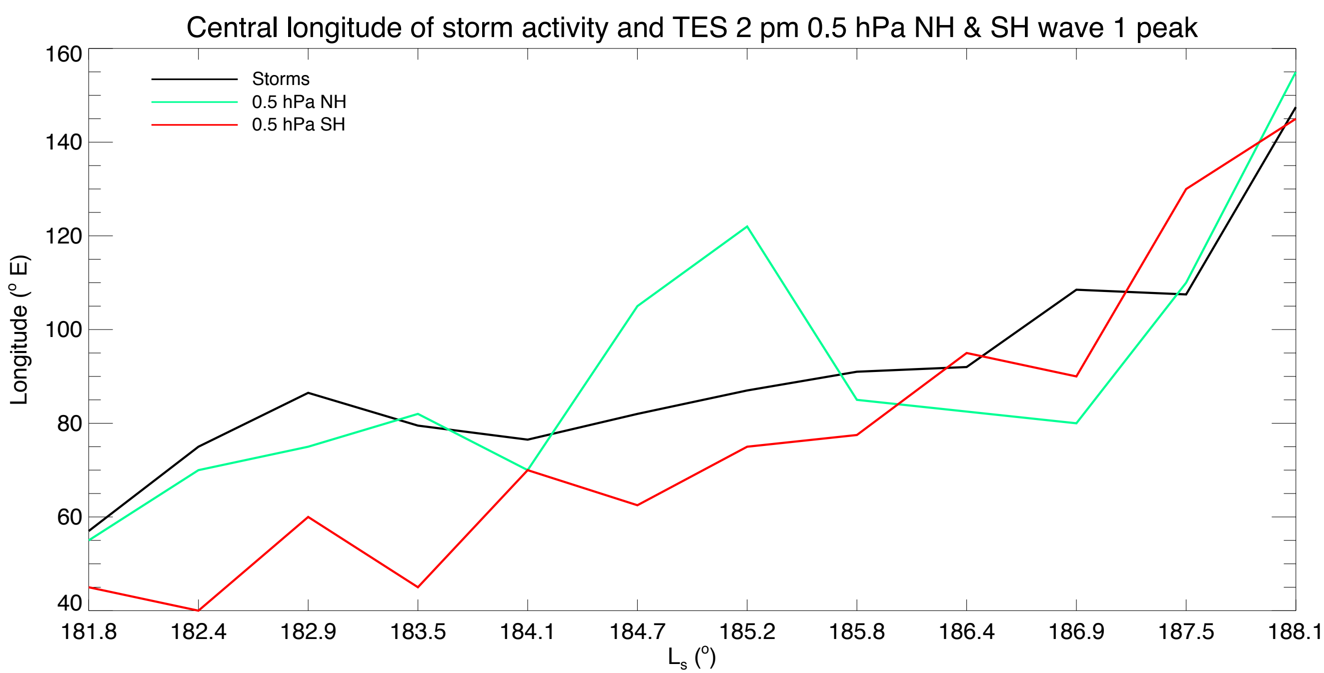

R12

Expansion phase

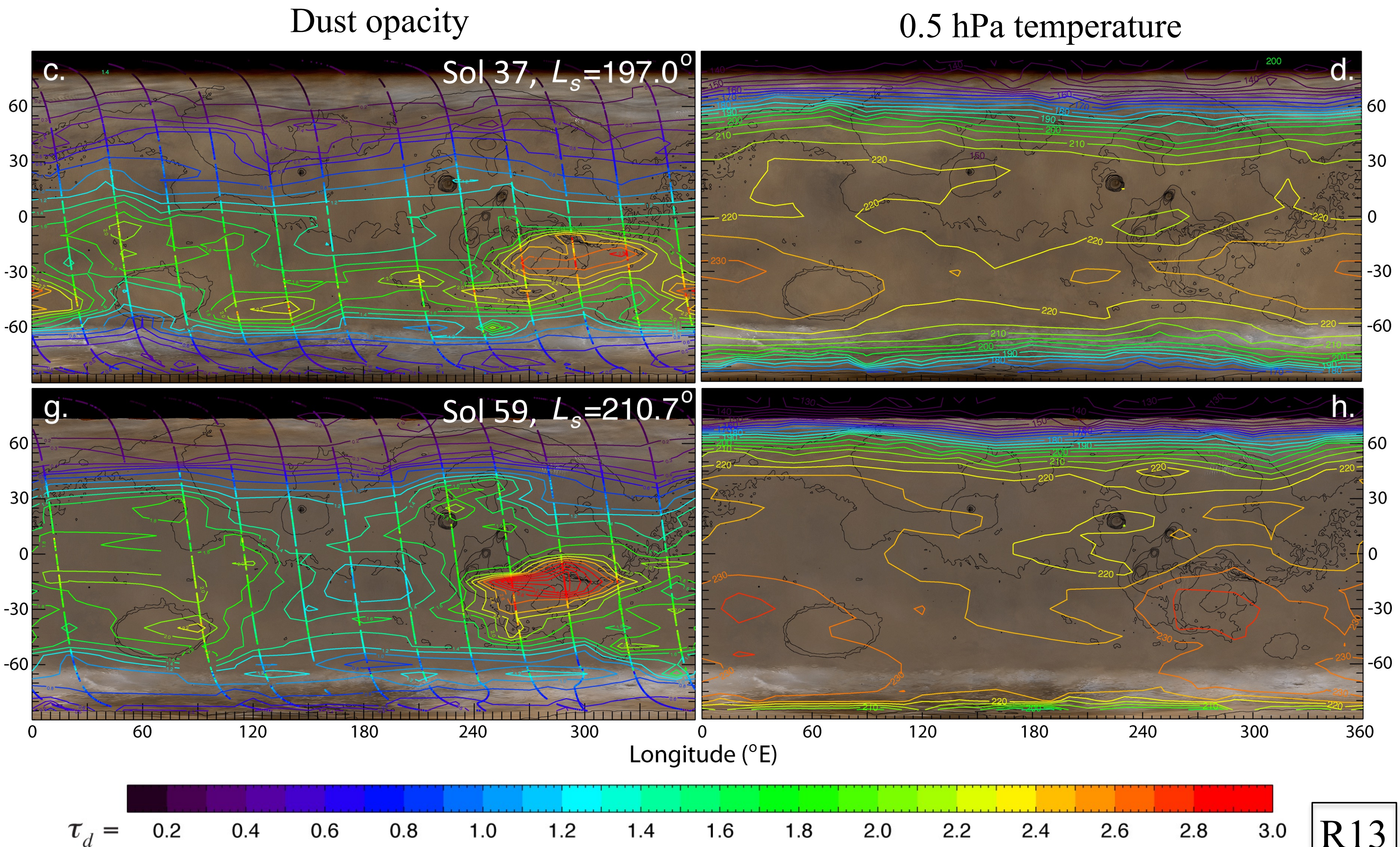

R13

TES Temperature tendency & dust cloud height estimates

The total day-to-day temperature change field, ΔT, is the sum of

- Radiative (thermodynamic) components: localized dust-induced forcing.
- Dynamical components: zonal and meridional circulations, thermal tides.

Assuming that radiative forcing is the dominant component, ΔT can be used as a proxy for first-order estimates of and constraints on dust cloud heights.

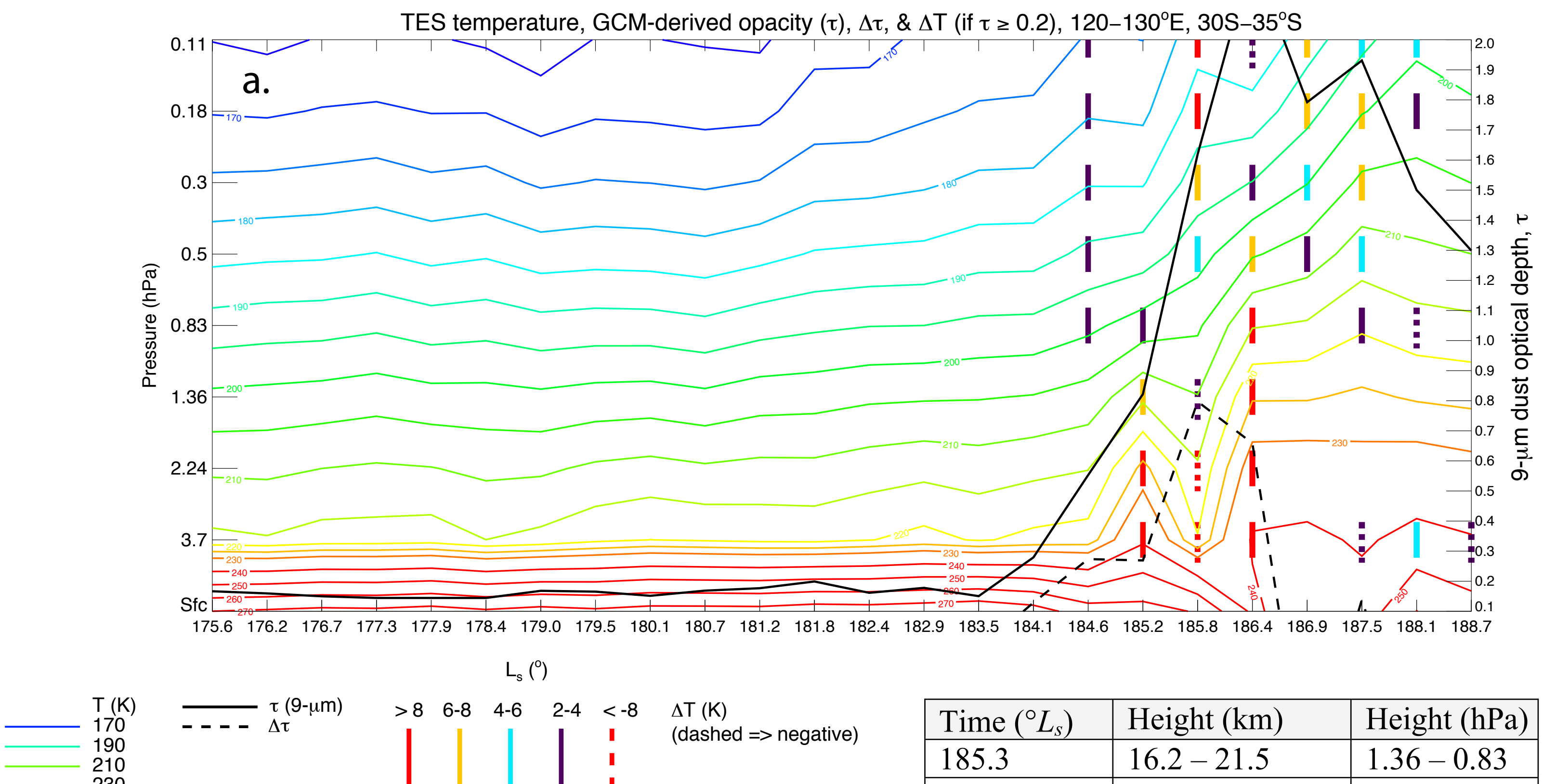

Time (°L_s)	Height (km)	Height (hPa)
185.3	16.2 – 21.5	1.36 – 0.83
185.9	27 – 38	0.5 – 0.18

R14

Synthesized dust maps

Problem:

- TES opacity retrieval reliability is partially a function of surface-air temperature contrast, with reliability diminishing as contrast approaches zero.
- Missing opacity data limits the reliability of MGCM simulations.

Method:

- Interpolate missing TES data from all available MGS data (Noble *et al.* 2011)
- MGCM-derived opacity estimates (Wilson *et al.* 2011)

Synthesized dust map, Hellas quadrant, L_s=187.5°

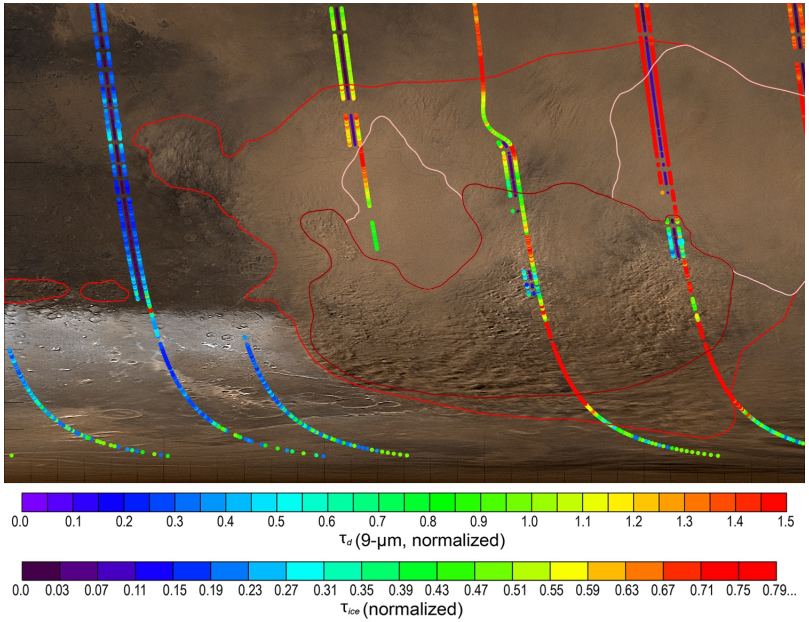

Gridded TES opacity

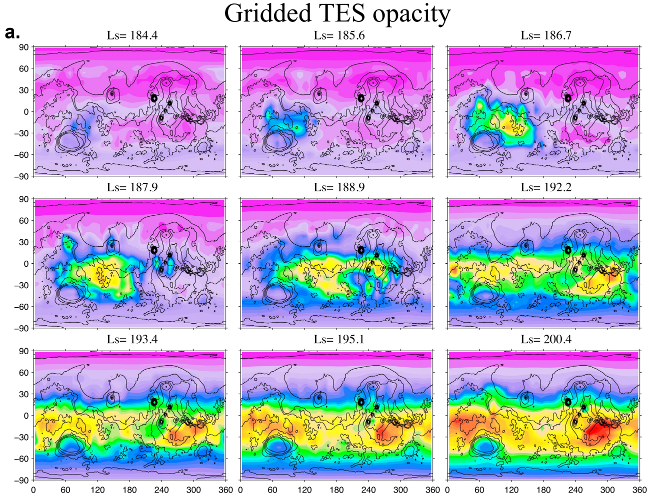

Synthesized opacity

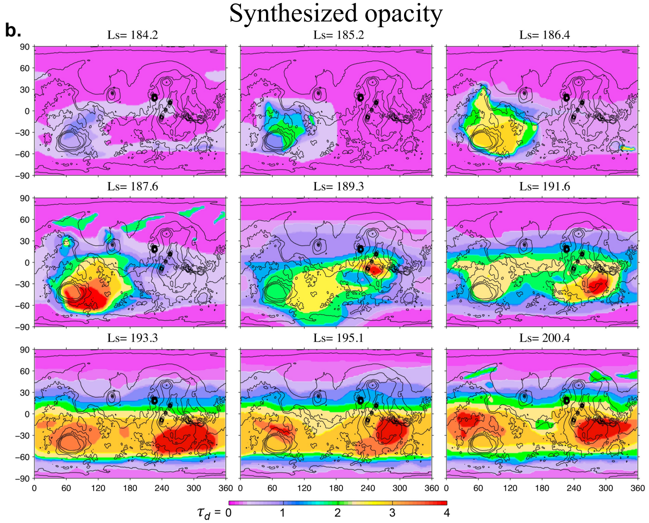

(Wilson *et al.* 2008, 2011)

Conclusions

We hypothesize that:

- Six eastward-traveling baroclinic eddies triggered the precursor storms due to the enhanced dust lifting associated with their low-level wind and stress fields.

- The sustained series of high-amplitude eddies in MY 25 was a factor in GDS occurrence that year.

~~~~~~~~~~~~~~~~~~~~~~

Our analysis has yielded important results regarding the dynamical response of the atmosphere to dust loading and the evolution of the dust storm.

Results from this investigation are being used to validate the NASA-Ames and NOAA GFDL MGCMs.
~~~~~~~~~~~~~~~~~~~~~~

Conclusions

- Our analysis has yielded important results regarding the dynamical response of the atmosphere to dust loading and the evolution of the dust storm. Results from this investigation have been used to validate the NASA-Ames MGCM.

- Integration of MGS data has increased our understanding of GDS dynamical processes and allowed us to develop an improved quantitative description of storm evolution that may be used to constrain both estimates of horizontal dust distribution and modeling of storm initiation and expansion.

- We are continuing to refine our dust opacity maps and use them as input into both the NASA and GFDL MGCMs. In future work we will present model results that relate the simulated circulation and atmospheric temperature and aerosol distributions to the available observations in an effort to better understand the underlying dynamics of the initiation and growth of the MY 25 GDS.

Committee

- Robert Haberle, *NASA-Ames Research Center*
- Alison Bridger, *San José State University*
- John Wilson, *NOAA GFDL*
- Eugene Cordero, *San José State University*

Collaborators

- Robert Haberle, *NASA-Ames Research Center*
- Alison Bridger, *San José State University*
- John Wilson, *NOAA GFDL*
- Jeffrey Barnes, *Oregon State University*
- Jeffrey Hollingsworth, *NASA-Ames Research Center*
- Jim Murphy, *New Mexico State University*

Data

- Mike Smith, (TES), *NASA-Goddard Space Flight Center*
- Bruce Cantor and Michael Malin, (MOC), *Malin Space Science Systems*
- Terry Martin, (MHSA), *NASA Jet Propulsion Laboratory*

References

Flammarion, C., 1892: *La planéte Mars et ses conditions d'habitabilité: Synthèse générale de toutes le observations*. Vol. I, Gauthier-Villars et Fils, Imprimeurs-Libraires de l'observatoire de Paris.

Haberle, R. M., 2003: Planetary Atmospheres: Mars. Encyclopedia of Atmospheric Sciences, J. R. Holton, J. A. Curry, and J. A. Pyle, Eds., Academic Press, 1745–1755.

Haberle, R. M., 1997: Mars: Atmosphere. Encyclopedia of Planetary Sciences, J. H. Shirley, and R. W. Fairbridge, Eds., Springer, 432–440.

Leovy, C., 2001: Weather and climate on Mars. *Nature*, **412**, 245–249.

Noble, J., *et al.,* 2011: Comparison of TES FFSM Eddies and MOC Storms, MY 24–26. *Mars Atmosphere Workshop 4*, Paris, France.

Owen, T., 1992: The Composition and Early History of the Atmosphere of Mars. Mars, H. H. Kieffer, B. M. Jakosky, C. W. Snyder, and M. S. Matthews, Eds., University of Arizona Press, 818–834.

Read, P. L., and S. R. Lewis, 2004: The Martian climate revisited: atmosphere and environment of a desert planet. Springer-Praxis Books, 326 pp.

Smith, M. *et al.,* 2000: Mars Global Surveyor Thermal Emission Spectrometer (TES) observations of dust opacity during aerobraking and science phasing. *Journal of Geophysical Research*, **105**, 9539–9552.

Wilson, R. J., R. M. Haberle, J. Noble, e*t al*., 2008: Simulation of the 2001 Planet-encircling Dust Storm with the NASA/NOAA Mars General Circulation Model. *Mars Atmosphere Workshop 3,* Williamsburg, VA.

Wilson, R. J., J. Noble, and S. J. Greybush, 2011: The derivation of atmospheric opacity from surface temperature observations. *Mars Atmosphere Workshop 4,* Paris, France.

Zurek, R. W., J. R. Barnes, R. M. Haberle, and J. B. Pollack, 1992: Dynamics of the atmosphere of Mars. Mars, H. H. Kieffer, *et al.,* Eds., University of Arizona Press, 835–933.

The end

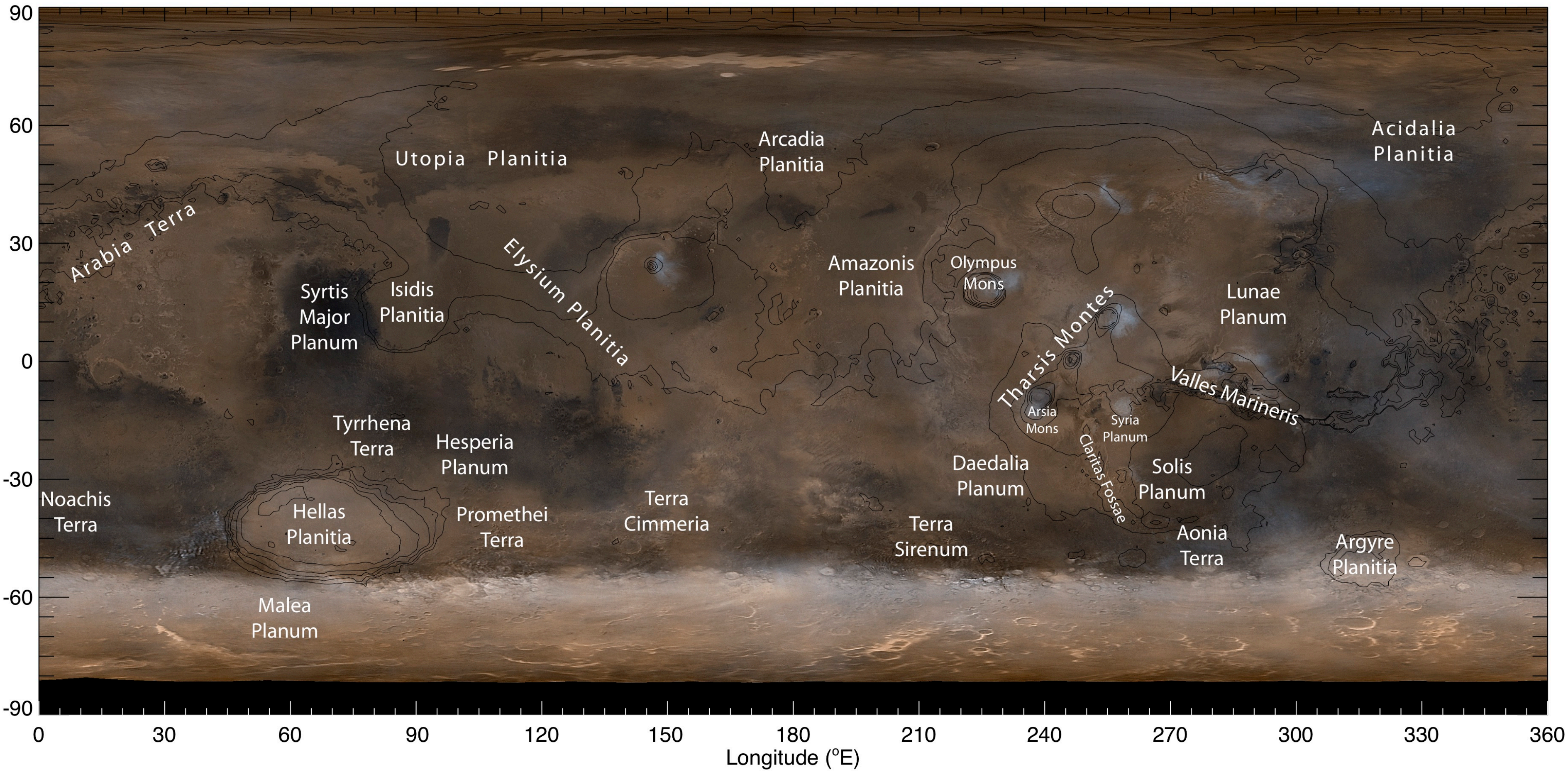
90
60
30
0
-30
-60
-90
0
30
60
90
120
150
180
210
240
270
300
330
360
Longitude (°E)
Utopia Planitia
Arcadia Planitia
Acidalia Planitia
Arabia Terra
Elysium Planitia
Amazonis Planitia
Olympus Mons
Syrtis Major Planum
Isidis Planitia
Lunae Planum
Tharsis Montes
Valles Marineris
Arsia Mons
Syria Planum
Claritas Fossae
Tyrrhena Terra
Hesperia Planum
Daedalia Planum
Solis Planum
Noachis Terra
Hellas Planitia
Promethei Terra
Terra Cimmeria
Terra Sirenum
Aonia Terra
Argyre Planitia
Malea Planum

History

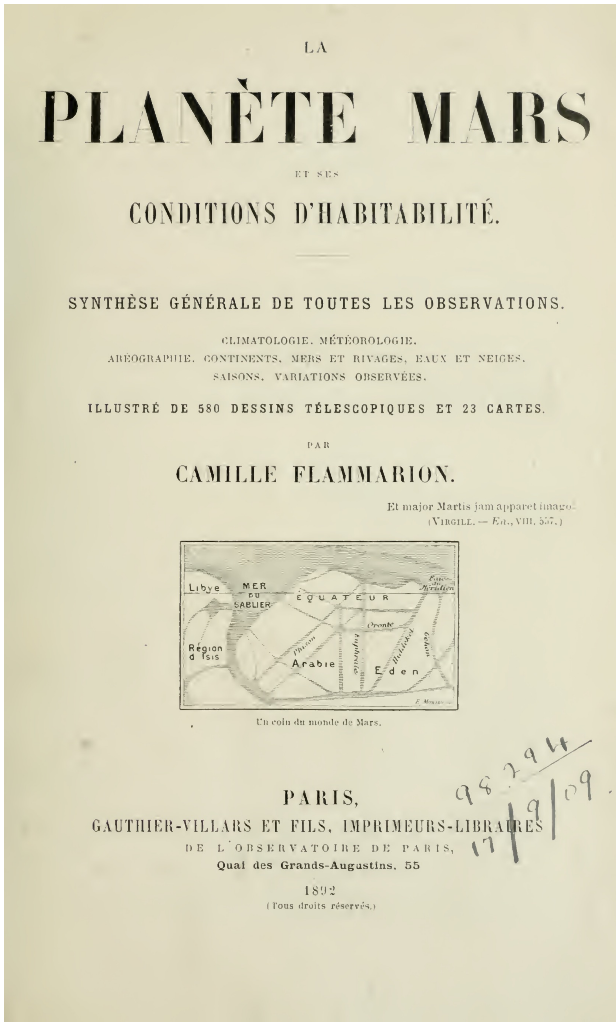
LA

PLANÈTE MARS

ET SES

CONDITIONS D'HABITABILITÉ.

SYNTHÈSE GÉNÉRALE DE TOUTES LES OBSERVATIONS.

CLIMATOLOGIE. MÉTÉOROLOGIE.
ARÉOGRAPHIE. CONTINENTS, MERS ET RIVAGES, EAUX ET NEIGES.
SAISONS. VARIATIONS OBSERVÉES.

ILLUSTRÉ DE 580 DESSINS TÉLESCOPIQUES ET 23 CARTES.

PAR

CAMILLE FLAMMARION.

Et major Martis jam apparet imago.
(VIRGILE. — Én., VIII, 557.)

Un coin du monde de Mars.

PARIS,
GAUTHIER-VILLARS ET FILS, IMPRIMEURS-LIBRAIRES
DE L'OBSERVATOIRE DE PARIS,
Quai des Grands-Augustins, 55

1892

(Tous droits réservés.)

Yellow-colored regions (“yellow clouds”) have been observed for ~ two centuries, first by Flaugergues in the late 1700s and early 1800s (Flammarion 1892), and later by Schiaparelli (1893, 1899), Flammarion (1892), and others.

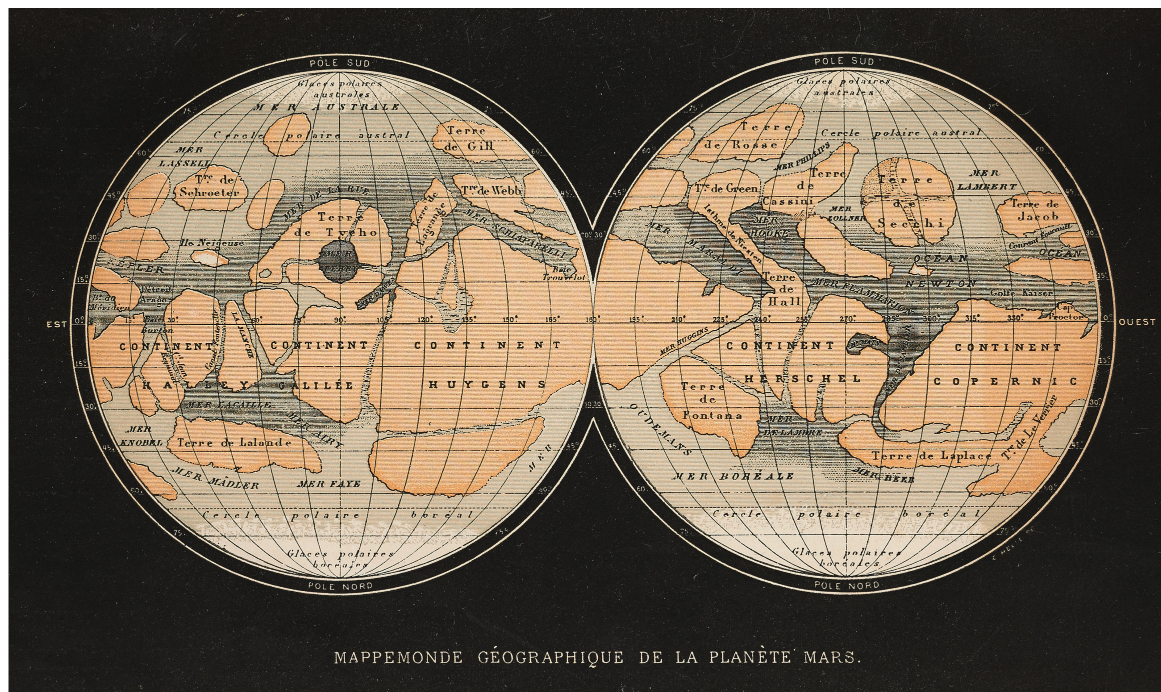

(Flammarion 1892)

Topography

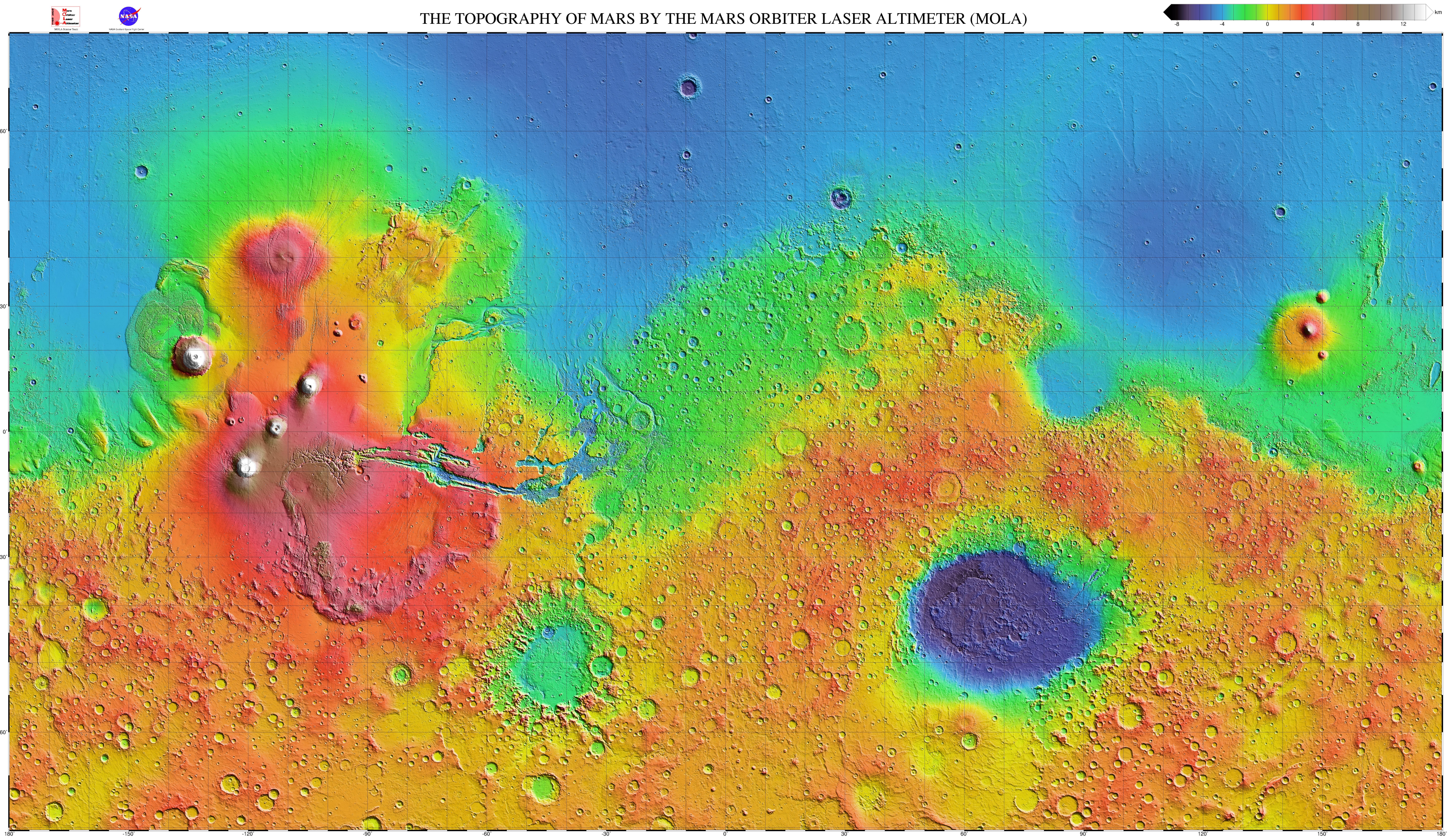
THE TOPOGRAPHY OF MARS BY THE MARS ORBITER LASER ALTIMETER (MOLA)
-8 -4 0 4 8 12 km
60
30
0
-30
-60
180 -150 -120 -90 -60 -30 0 30 60 90 120 150 180

Martian orbit and seasons

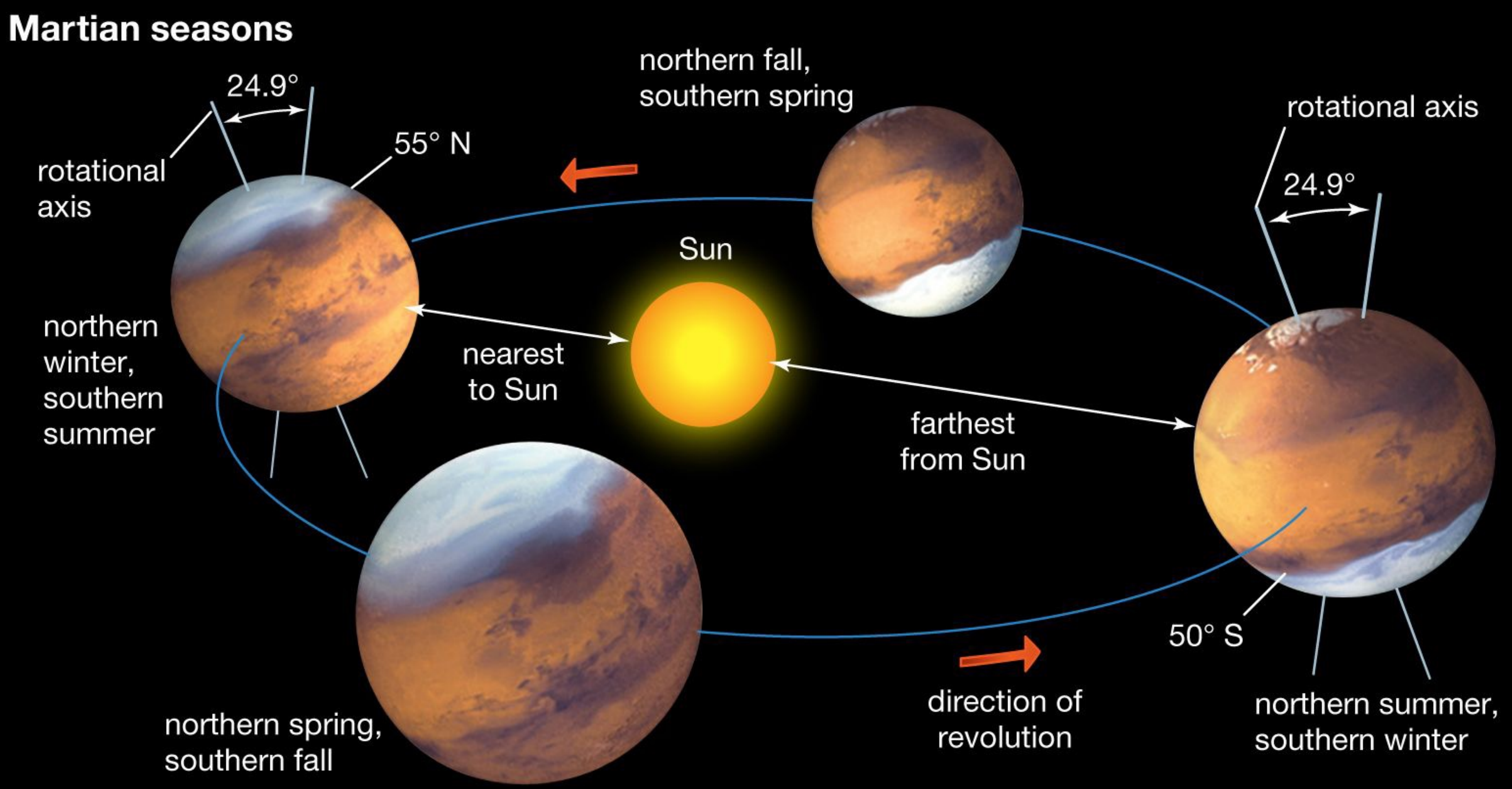

Atmospheric constituents

Composition	Constituent
95.32%	Carbon dioxide
2.7%	Nitrogen
1.6%	Argon
0.13%	Oxygen
0.07%	Carbon monoxide
0.03%	Water vapor
Trace:	Neon, krypton, xenon, ozone, methane

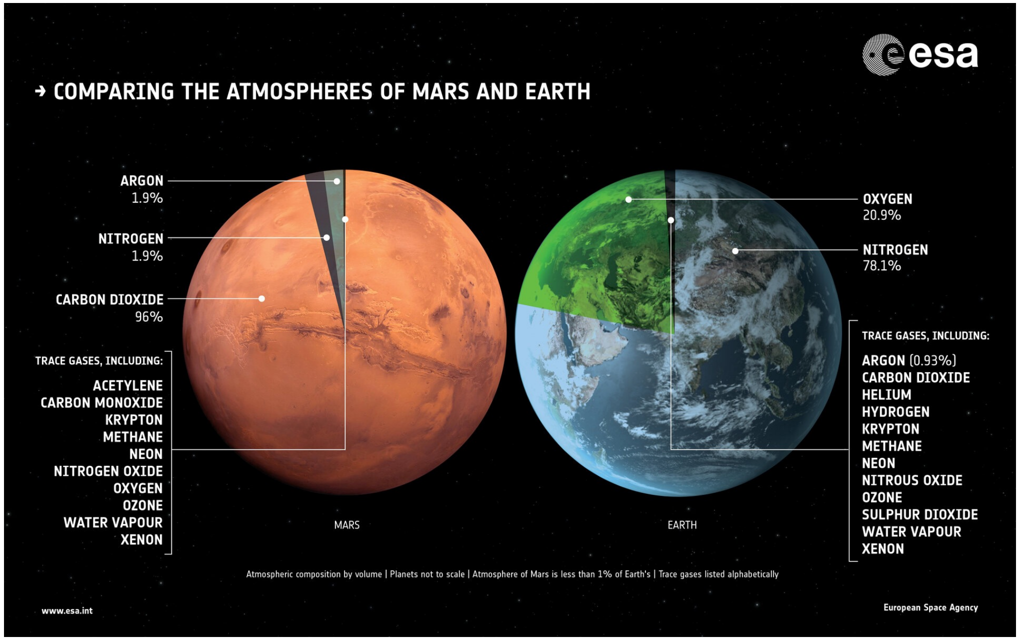

Vertical structure of the Martian atmosphere

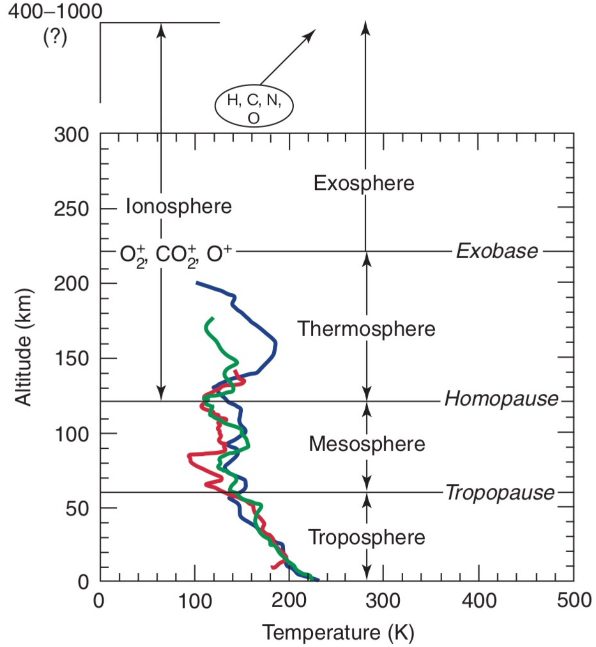

Figure 1 Vertical structure of the Martian atmosphere. Colored curves are temperatures inferred from deceleration measurements aboard the *Viking 1* (blue), *Viking 2* (green), and *Pathfinder* (red) landers.

(Haberle 2003)

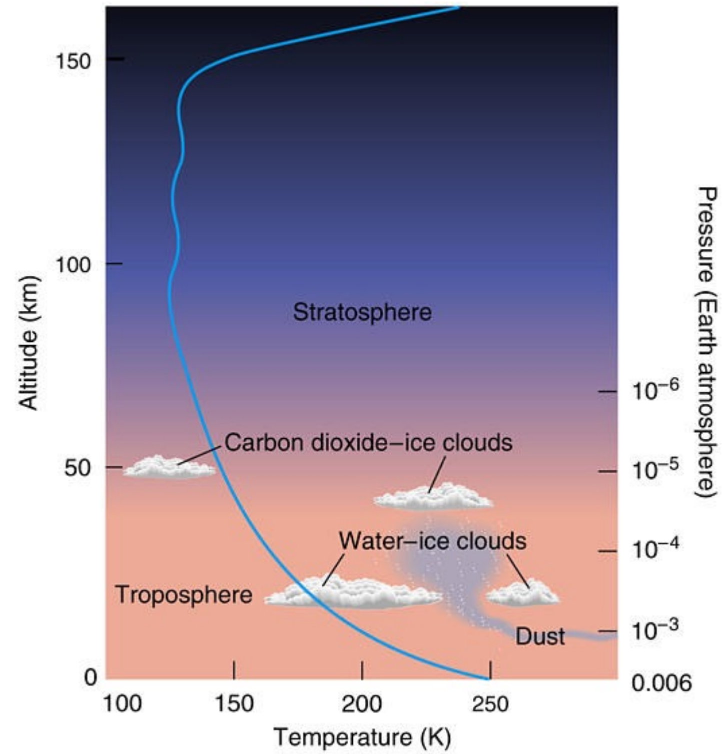

Blackbody emission & temperature

- Surface temperatures range from 150 K to 275 K.
- Although the Martian atmosphere is composed primarily of CO_2 (95%), greenhouse warming raises temperatures by only 5 K above the radiative equilibrium temperature.
- The atmosphere only absorbs radiation in a narrow band of the spectrum.
- 40% seasonal change in insolation, compared with 6% for Earth.

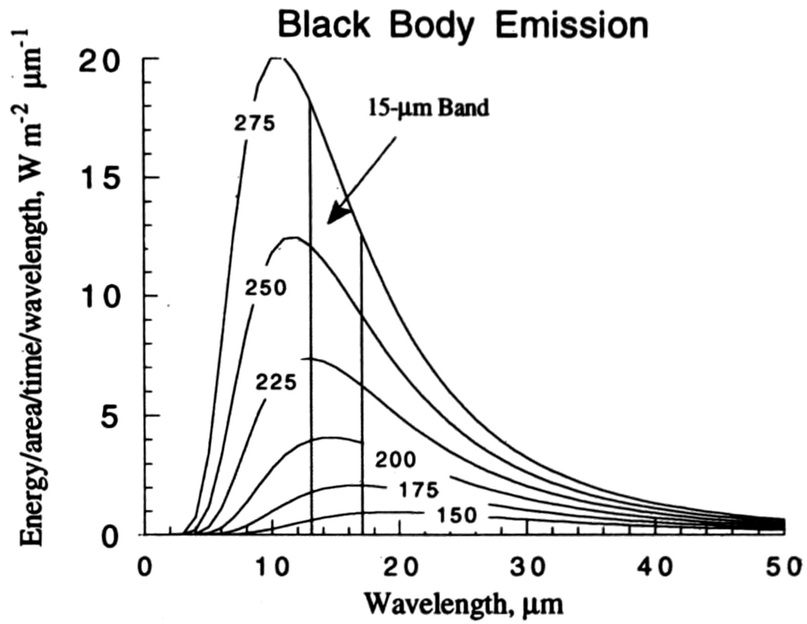

Figure M24 Blackbody emission as a function of wavelength for a range of temperatures representative of the Martian surface. CO_2 is the principal infrared absorbing gas in the Martian atmosphere and the approximate width of its 15-μm absorption feature is indicated.

(Haberle 1997)

Greenhouse effect

$$T_e = \left(\frac{S_0 \left(1 - A_p\right)}{4\sigma} \right)^{1/4}$$

T_e = Effective Temperature = 210 K

T_s = Average Surface Temp = 215 K

A_p = Planetary Albedo = 0.26

S_0 = Solar Flux = 590 W m^{-2}

σ = Stefan-Boltzman Constant

$$T_s - T_e = 5 \text{ K}$$

Surface pressure

- 1–9 hPa (mean ≈ 6 hPa)
- Function of season and altitude

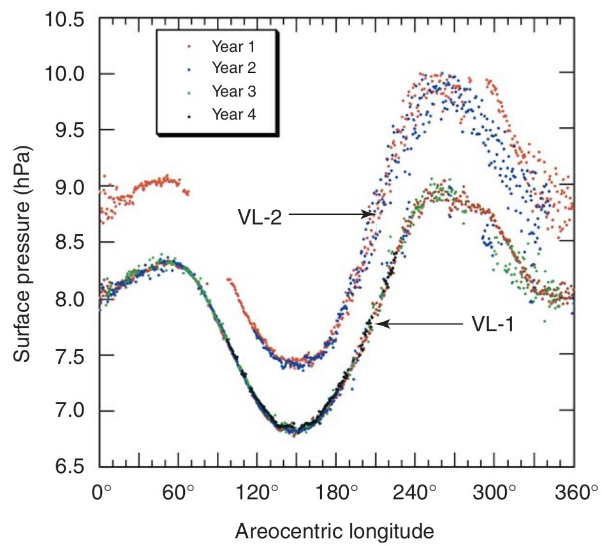

Figure 5 Seasonal variation of the daily averaged surface pressure on Mars measured by the *Viking Landers*.

(Haberle 2003)

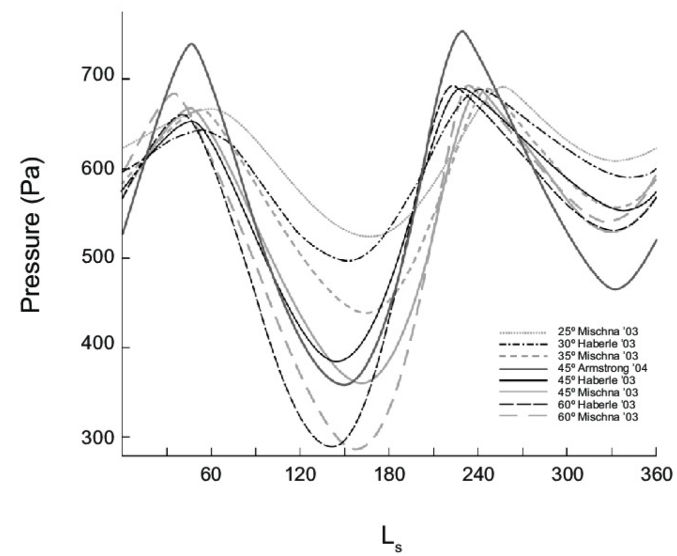

Thermal Emission Spectrometer (TES)

- TES is an interferometric spectrometer that measures thermal emission in the IR spectrum from 6–50 μm (wavenumbers 1600–200 cm^{-1}).
- There are six detectors yielding a spatial resolution of ~3 x 9 km on the surface (Smith *et al.* 2002).
- Spectral data are used to retrieve the following quantities:
  - temperature (surface and atmospheric)
  - optical depth (dust and water ice aerosol)
  - water vapor column abundance (Smith *et al.* 2000)
- Atmospheric thermal retrievals were obtained from 3.7–0.01 hPa, approximately 5.4–70.4 km.

We refer to 9-μm (IR) dust optical depth hereafter as 'opacity' (τ_d). All opacity retrievals have been normalized to remove the effects of topography.

Thermal emission spectra

Atmospheric temperature profiles $T(p)$ are obtained from thermal emission spectra within the CO_2 absorption band centered at 15-μm (550–800 cm^{-1}).

Atmospheric dust has absorption bands between 800–1300 cm^{-1} and 300–550 cm^{-1}.

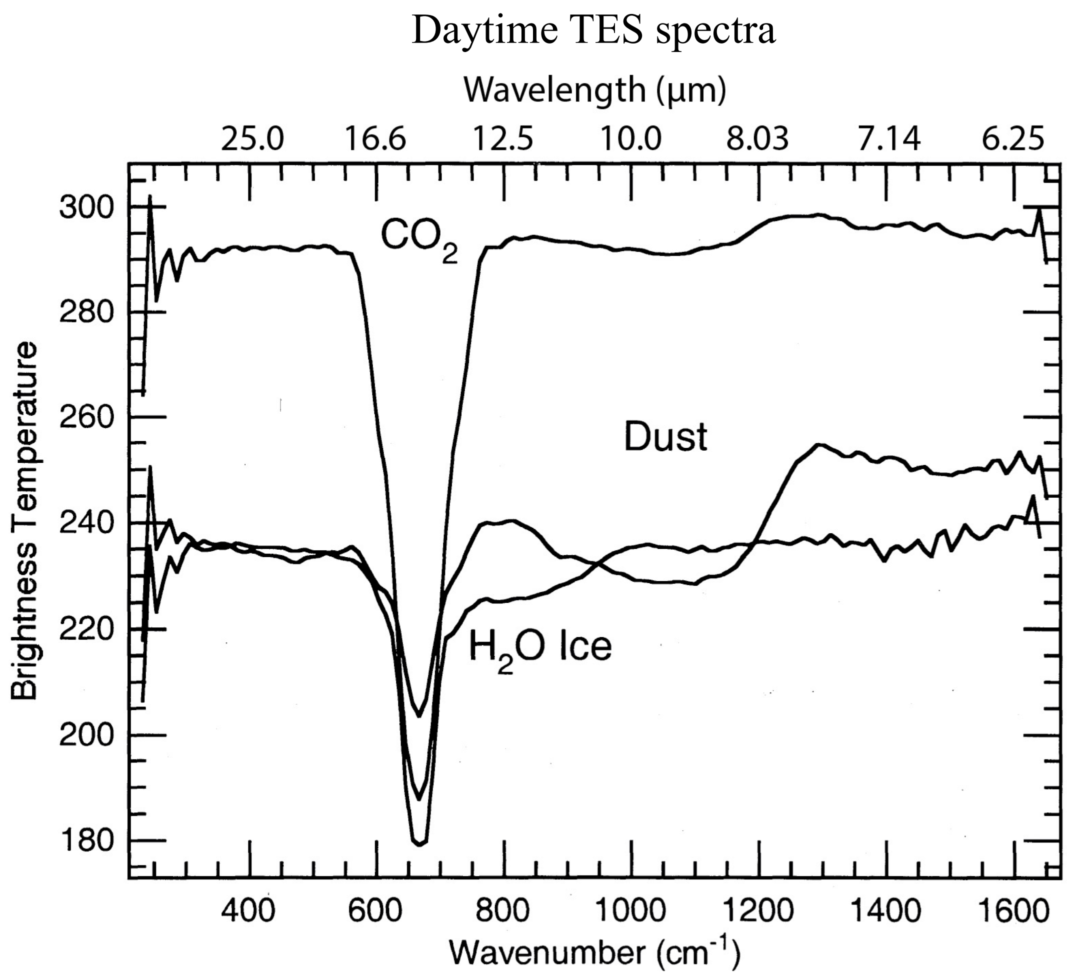

(Smith *et al.* 2000)

Thermal Emission Spectrometer

Radiance $I(\mu,\nu)$ measured by TES at the top of the atmosphere is formulated as

$$I(\mu,\nu) = \varepsilon(\nu)B(\nu,T_s)Tr(\mu,\nu,z_s) + \int_{z_s}^{z_t} B[\nu,T(z)]\frac{\partial Tr(\mu,\nu,z)}{\partial z}dz$$

After an atmospheric temperature retrieval has been calculated, an opacity retrieval is calculated with the following radiative transfer equation:

$$I_{\text{comp}}(\nu) = \varepsilon(\nu)B[T_{\text{surf}},\nu]e^{-\tau_0(\nu)/\mu} + \int_0^{\tau_0(\nu)} B[T(\tau),\nu]\,e^{-\tau/\mu}d\tau$$

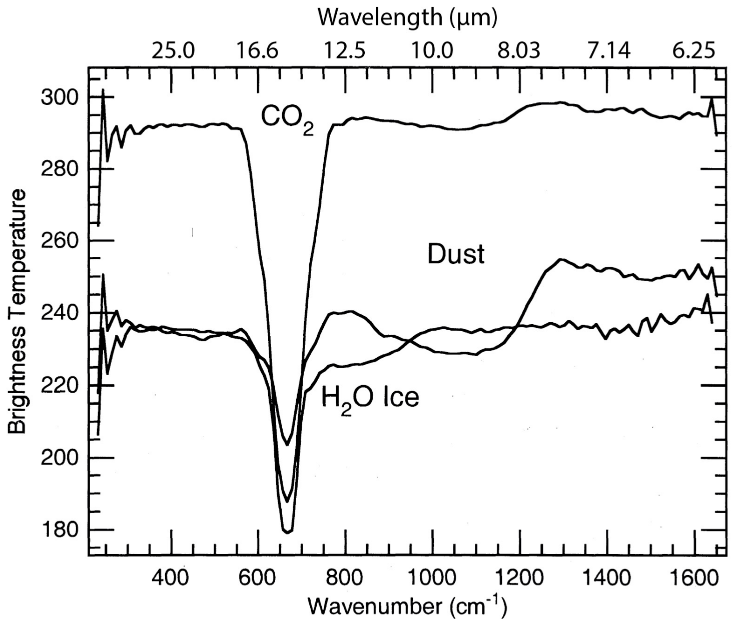

Daytime TES spectra

(Smith *et al.* 2000)

Fast Fourier Synoptic Mapping

- FFSM is a spectral analysis method that creates synoptic maps from asynoptic data, maintaining full space-time resolution without distorting or smoothing higher frequency (~1–3 sols) weather signals.
- This process removes the time mean, zonal mean, and westward diurnal tide.

Mars Orbiter Camera

- MOC consists of three push-broom cameras:
  - a single, high-resolution narrow-angle (NA) camera (500–900 nm).
  - two lower-resolution wide-angle (WA) cameras with red (575–625 nm) or blue (400–450 nm) band passes.

- The push-broom method constructs images one line at a time as opposed to capturing a single frame.

- MOC DGMs were created by map projecting (cylindrical) and mosaicking 12–13 global swaths (WA) (both red and blue band passes) of all daytime orbits.

- Each DGM is 3600 x 1800 pixels, with 10 pixels degree^{-1} resolution.

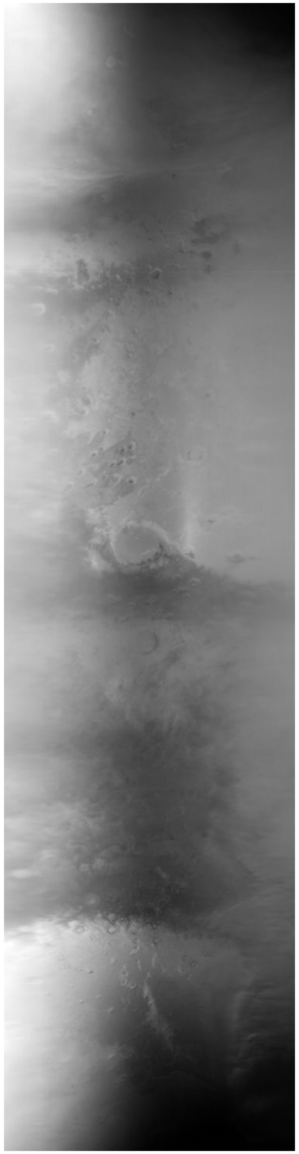

Mars Horizon Sensor Assembly

- MHSA is an MGS engineering instrument that measures 15-µm CO_2 band emission to monitor the limb in order to adjust spacecraft pitch and roll alignment.
- Atmospheric temperatures can be simultaneously derived from measurements made in four quadrants: aft (Q1), forward (Q2), right (Q3) and left (Q4). These are made at three local times each night/day: 2 am/pm (Q1 and Q2), 12:30 am/pm (Q3/Q4), and 3:30 am/pm (Q4/Q3) respectively.
- MHSA uses a broad weighting function that averages a region of the atmosphere 10–40 km above the surface.
- Advantages of MHSA data, from a meteorological perspective, include greater longitudinal and temporal coverage.
- MHSA data are also valuable because they contain continuous measurements throughout a several sol period (L_s=189.7–191.4°) of missing TES data.

TES FFSM eddies, 3.7 hPa, 60° S, MY 26, L_s=175.39–192.78°

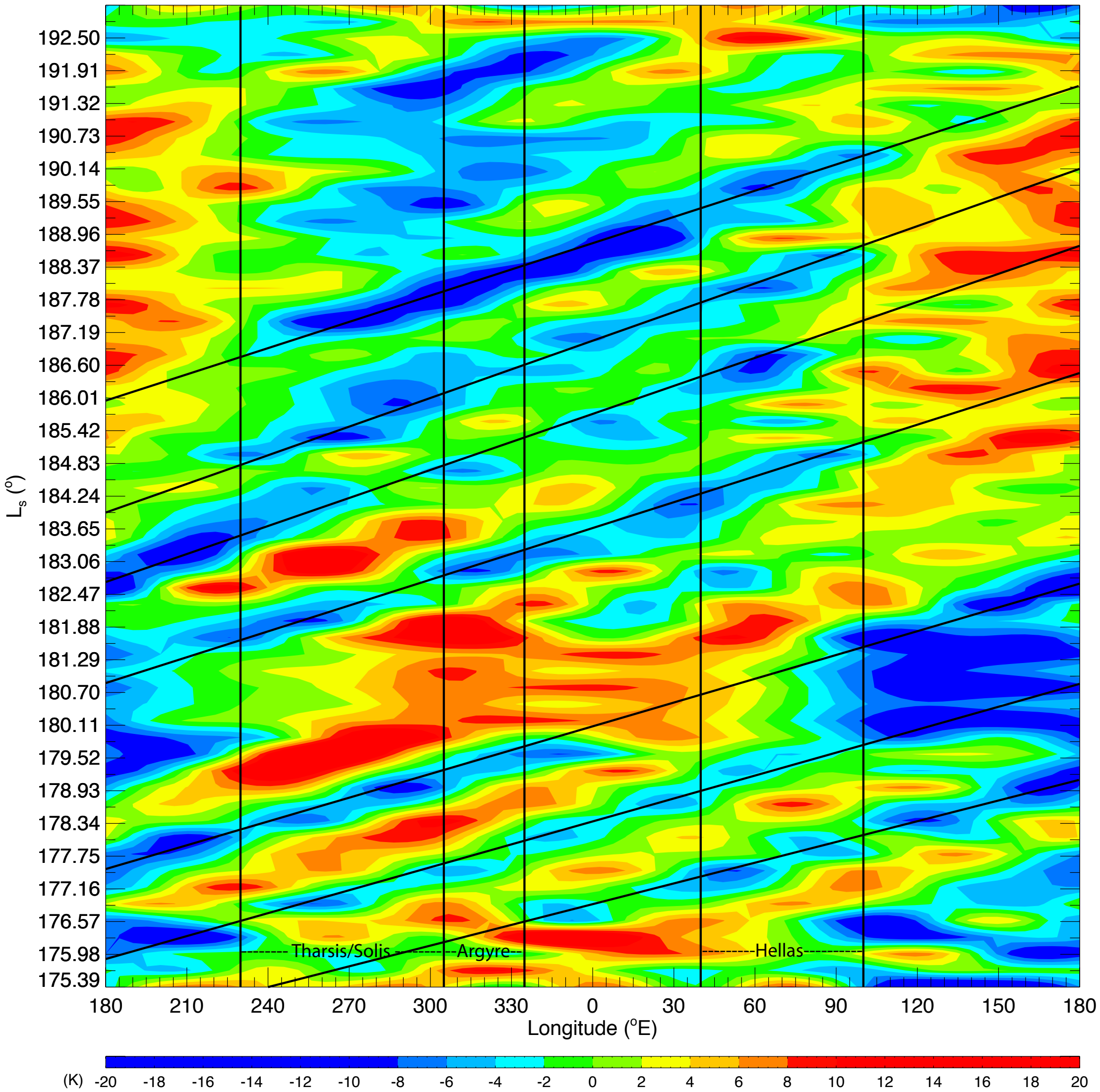

Different seasonal regime than MY 24 & 25.

Although some coherent transient eddies are visible in the storm zone described above, a strong stationary wave is evident.

Cold centers appear to dominate the 90–220° E longitude corridor from L_s=175–183°, followed by a polarity switch to warm centers from L_s=183–192°.

Several strong-amplitude eddies propagate into Hellas during L_s=183–190°.

Phase speed and periodicity

- **Global phase speed**: We subjectively defined globally-coherent eddies and calculated their phase speed, *c*, using:

$$c(x)=\Delta x/\Delta t,$$

where $\Delta x = (r_{eq} \cdot \cos\varphi) \cdot \Delta\lambda$, r_{eq} is planetary radius, φ is latitude, λ is longitude, and t is time at 180° E.

- **Period**: We estimated MY 24–26 eddy periodicities, *P*, in Hellas from FFSM longitude-time plots.

~ L_s (°): eddy at 60° E	Eddy #	*c* (m/s) global MY 24	*c* (m/s) global MY 25	*c* (m/s) global MY 26	*P* (sols) Hellas MY 24	*P* (sols) Hellas MY 25	*P* (sols) Hellas MY 26
176.5	**E1**	12.8	13.8				
178.0	**E2**	13.4	14.5	15.6	2.7	2.8	
179.3	**E3**	14.1	14.8	14.3	2.6	2.5	2.8
181.0	**E4**	14.5	13.1	13.8	2.8	3.0	2.9
182.7	**E5**	15.2	13.5		2.7	2.9	
184.6	**E6**	16.0	13.8	12.9	2.5	2.8	
186.3	**E7**	13.8	13.2	11.8	2.9	3.3	3.7
	Mean:	14.3	13.8	13.7	2.7	2.9	3.1

Eddy power spectra

Periodicities were also calculated by Fast Fourier Transform in IDL using:

$$F(u) = \frac{1}{N} \sum_{x=0}^{N-1} f(x) e^{-i2\pi u \frac{x}{N}}$$

where $F(u)$ is the discrete Fourier transform of an N-element, one-dimensional function, $f(x)$.

Power spectra for MY 24–25 Hellas (40–100° E, 60° S) eddies from L_s=165–188° show a dominant periodicity of ~3.5 sols for both years and values, along with moderately high adjacent amplitudes from 2.5–3.0 sols.

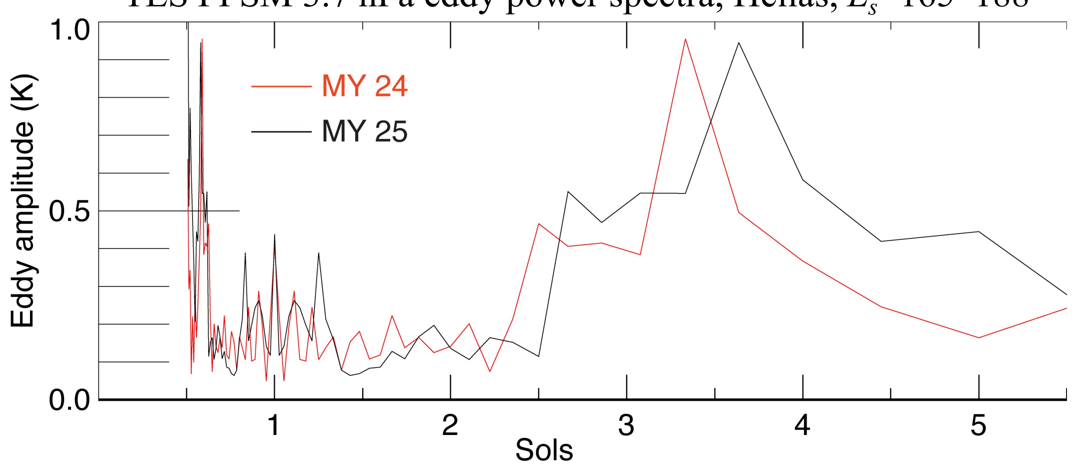

Synthesized dust maps

- TES opacity retrieval reliability is partially a function of surface-air temperature contrast, with reliability diminishing as contrast approaches zero.
- As a result, data from the meteorologically-significant periods of lifting onset and expansion in both Hellas and Claritas are unreliable.
- We believe that an improved opacity "sequence" would increase the credibility and reliability of numerical simulations.
- We produced two synthesized dust maps (SDM): column opacity and structured opacity.
  - Column opacity maps estimate atmospheric column opacity at each grid point from a range of 15 possible levels ($\tau_d = 0.2, 0.4, 0.6, \ldots, 3.0$).
  - Structured opacity maps delineate latitude-longitude boundaries where cloud top morphology is visibly structured. These regions are suggestive of convective activity and possibly of active lifting.
- Column opacity maps were created by hand and with MGCM-derived opacity.

Synthesized dust maps

Maps of MY 25 structured dust activity in Hellas. Orbits: normalized TES 9-µm dust opacity, TES H_2O ice opacity, & MGCM-derived dust opacity respectively

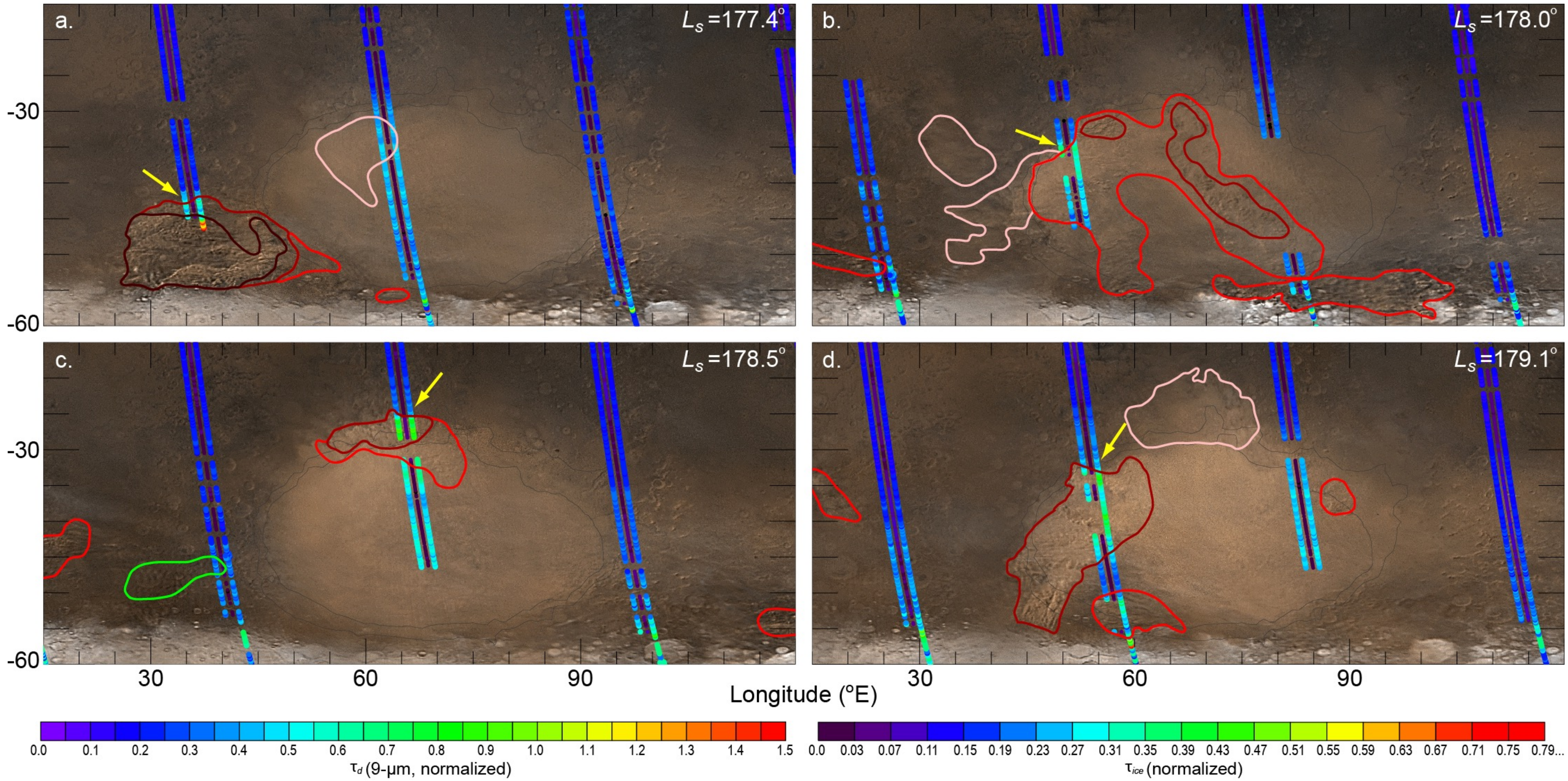

Synthesized dust maps

Map of structured dust activity, MY 25, $L_s = 186.4°$. Orbits: TES 9-μm dust opacity, TES H_2O ice opacity, and MGCM-derived dust opacity respectively